DTU Library

Canadian and Danish investigations on corrections of collector efficiency depending on fluid type, flow rate and collector tilt

Bava, Federico; Furbo, Simon; Brunger, Alfred

Link back to DTU Orbit

Canadian and Danish investigations on corrections of collector efficiency depending on fluid type, flow rate and collector tilt

Federico Bava

Simon Furbo

Alfred Brunger

Report

DTU Civil Engineering
Department of Civil Engineering

Canadian and Danish investigations on corrections of collector efficiency depending on fluid type, flow rate and collector tilt

Federico Bava & Simon Furbo, Technical University of Denmark and
Alfred Brunger, EXOVA, Canada

Introduction

In its basic form, a solar thermal collector is designed to intercept solar radiation, absorb that radiation to convert it into heat energy, and then deliver that heat to a heat transfer fluid. Therefore, the performance of a solar thermal collector is influenced by all variables that affect either the optical or the thermal properties of the collector. For example, the incidence angle of solar radiation onto the solar collector can affect the optical performance of the collector. While typically not a strong factor for solar thermal collectors, the changing spectral quality of sunlight with changing atmospheric conditions can influence the fraction of the incoming solar radiation that gets transmitted and absorbed by the collector. Tilt angle, especially for glazed flat plate collectors, affects internal and external convective heat transfer coefficients, and thus influences collector thermal performance. Heat transfer fluid flow rate and fluid thermal properties influence the heat transfer coefficient inside the fluid passages of the collector, and thus influence the collector efficiency.

Solar collector data sheets released by test institutes usually state the collector efficiency only for one operating condition, which can differ significantly from those actually used in solar heating systems, so the actual thermal performance of the collector cannot be known in advance. This study focused on the experimental test of three solar collectors, in different conditions of flow rate, collector tilt angle and fluid type, to verify the influence that each parameter has on the collector efficiency and access the error which is introduced when the collector efficiency from the technical data sheet is used in place of one evaluated under more realistic operating conditions.

In the first part of the study, the thermal performance of a single flat plate collector was measured with two different heat transfer fluids, two different tilt angles, and three different fluid flow rates. Tests were conducted with twelve different combinations of these three parameters, and the results have been used to quantify the effects of these variables on the thermal performance of the solar collector. The

results of the tests are presented in detail in the section "Canadian investigations".

In the second part of the study (section "Danish investigations") two large solar collectors were investigated, more specifically the models HT-SA 35-10 and HT-A 35-10, manufactured by the Danish company ARCON Solar A/S. These collectors have large aperture area (about 12.5 m^2) and they are installed in large number in solar collector fields for district heating purposes. This kind of installation is very common in Denmark, where more than 50 collector fields could be found at the end of 2014, the largest of which has a collector area of 37,573 square meters (Dronninglund field).

The two ARCON collectors were identical with the only difference being a FEP (fluorinated ethylene propylene) foil interposed between the absorbing plate and the glass cover in the model HT-SA. The presence of the FEP foil is expected to reduce the convection losses, as the air between the absorber and the glass circulates in two different layers of convective cells, one above and the other below the foil. The heat losses from the collector cover are therefore lower than in the collector without foil, due to the additional thermal resistance given by the convective heat transfer coefficient between the air and the FEP foil. Nevertheless, as the foil is not completely transparent, it slightly reduces the solar irradiance reaching the absorber. Consequently, there is a certain operating temperature below which the collector without foil performs better than the other, as the transmittance of the cover plays a more significant role than the thermal losses.

The technical specification sheets (Arcon Solar, 2010; SP Technical Research Institute of Sweden, 2011) state the collector efficiency when a 25 litres min^{-1} flow rate of pure water is supplied to a 60° tilted collector, conditions which are very unlikely to be found in a Danish solar collector field. For this reason, the two collectors were tested at different flow rates and tilt angles, using a mixture of propylene glycol (PG) and water with a mass concentration of 40% PG. In fact, the efficiency of a solar collector is influenced by the volume flow rate, as shown by Chiou (1982) and Wang and Wu (1990) for vertical pipe collectors and by Fan and Furbo (2008) for horizontal pipe collectors. The influence of the tilt on collector efficiency was investigated by Furbo and Holck (1995).

The experimental determination of the collector efficiency equation is of key importance when assessing the actual performance of the collectors in certain operating conditions. As experimental tests are usually time consuming and expensive, it may be useful to have a model that is able to estimate the collector efficiency, so that it can be used to predict its value also under conditions that differ from those tested. In this study, such a model was created in Soleff, software developed at Technical University of Denmark (Rasmussen and Svendsen, 1996), and compared to the experimental measurements. The results of the simulation models and the comparison with the experimental efficiencies are presented in the section "Analyses on prediction methods to determine efficiencies for collectors in operation in solar collector fields".

Chapter 2: Canadian investigations

2.1 Description of the investigated solar collector

The collector selected for the tests was the model of collector used in the Drake Landing Solar Community project in Alberta, Canada. Detailed information for the collector is listed below. A photograph of the collector under test in the NSTF is shown in Figure 2.1.

Manufacturer: EnerWorks Inc., Canada
Collector Model: COL-4X8-NL-SGI-SH10
Serial Number: 1202064
Collector Type: Glazed flat plate, liquid-heating, serpentine flow pattern
General Construction[1]:   Carbon steel frame w/Galvalume coating, aluminum back sheet.
Flow Pattern: Serpentine with internal headers
Serpentine tubes[1]:   10 mm OD (9 mm ID) copper tube
Internal headers[1]:   22 mm OD (21 mm ID) copper pipe
Cover Plate[1]:   AFG Solatex tempered glass, 3.3 mm thick, sand pattern
Absorber Material[1]:   0.5 mm thick aluminum
Absorber Coating[1]:   Miro-therm coated front surface, corrosion resistant nickel based coating on rear surface.
Gross Dimensions: 2.442 m x 1.175 m; Area: 2.869 m²
Insulation[1]:   1-3/8" thick mineral wool back insulation, protected by 0.016" thick aluminum sheet on the outside. 1" thick polyisocyanurate foam edge insulation.
Dry Weight[1]:   50 kg.
Mounting Details: Attached to test frame with Unistrut

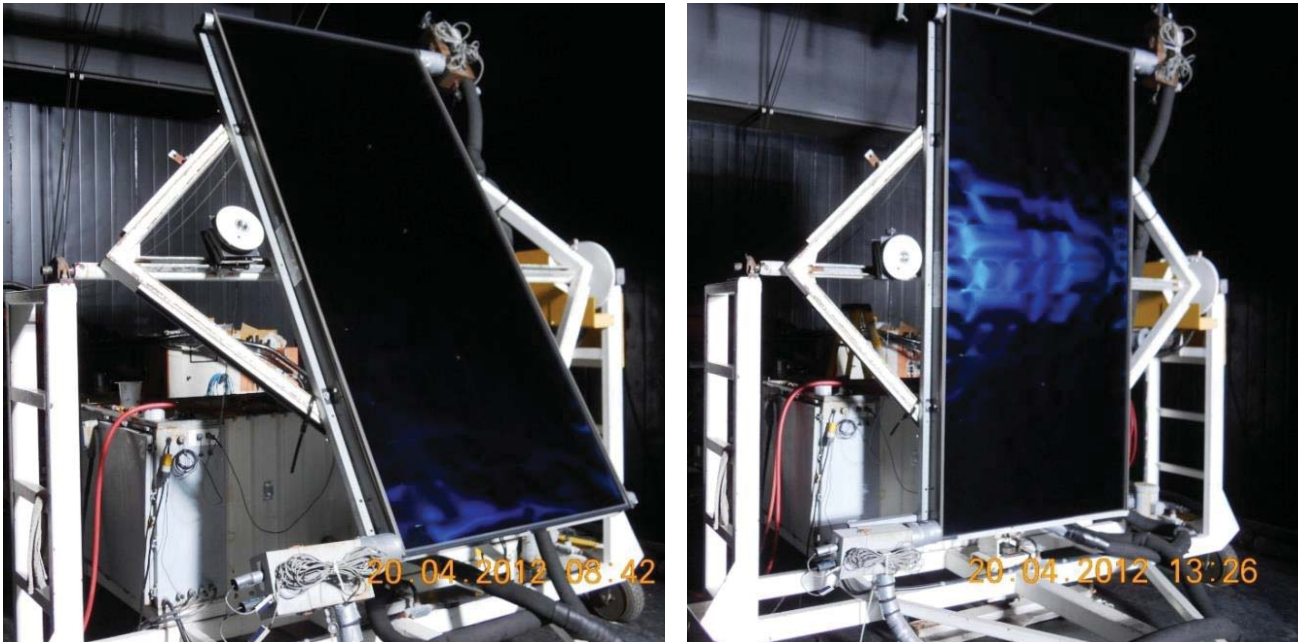[1] Information supplied by the manufacturer.

Figure 2.1: Test collector mounted in the solar simulator chamber, showing the two different mounting positions.

2.2 Test facility and test conditions

The Canadian test plan was designed to quantify the effects of tilt angle, flow rate, and fluid type on the efficiency of a liquid-heating glazed flat plate collector. All the tests were carried out indoors in the large area solar simulator at the National Solar Test Facility of Canada (NSTF), located at the Exova Technology Centre in Mississauga, Ontario. The solar simulator shines into an environmental chamber where the test collector is mounted. Wind generators on either side of the solar irradiance window provide constant wind speed conditions with turbulence characteristics designed to match natural outdoor wind. Air temperature, irradiance and wind speed can be controlled to various setpoints, and held constant during testing.

To reduce the number of parameters to vary and analyze, we endeavored to keep the solar irradiance and wind speed constant during the tests. With three independent variables considered for the tests, and multiple levels desired for each of the parameters, a full factorial experiment with three levels of each parameter would require 27 different thermal performance tests on the same collector. To save on testing resources while still covering the main objectives of our tests, we reduced the number of levels of tilt angle and fluid type, as shown in Table 2.1.

For all the tests, the solar irradiance was kept at 810 W/m^2 $\pm$ 10 W/m^2 and the wind generators were kept running a constant speed. An unintended consequence of keeping the wind generators set at the same RPM was that the average wind speed over the face of the collector was lower when the collector was vertical than when the collector was tilted back to 60 degrees from horizontal. For the vertical

collector tests, the average wind speed was 2.6 m/s. For the tests with the collector at a 60 degree tilt, the average wind speed was 3.9 m/s. As a result, the effect of tilt angle was confounded with the effect of wind speed in these tests.

Table 2.1: Summary of Test Plan for Canadian Investigations

Test No.	Test Fluid	Flow Rate (L/min per collector)	Flow Rate (kg/s per collector)	Tilt Angle (degrees)	Order to Perform Test
1	Water	0.18	0.003	60	C
2	Water	1.20	0.020	60	D
3	Water	3.44	0.057	60	A
4	Water	0.18	0.003	90	F
5	Water	1.20	0.020	90	E
6	Water	3.44	0.057	90	B
7	50% PG	0.18†	0.003'	60	J
8	50% PG	1.2†	0.02'	60	I
9	50% PG	3.44†	0.0573'	60	G
10	50% PG	0.18*	0.003*	60	H
11	50% PG	1.2*	0.02*	60	K
12	50% PG	3.44*	0.0573*	60	L

† For these three tests, the mass flow rate was kept the same as the setting for water.
* For these three tests, the product of mass flow and thermal capacitance (m•Cp) was matched to the (m•Cp) used for the corresponding tests with water.

Three flow rates were chosen to try to cover as wide a range as possible, while keeping the solar irradiance the same for all tests. Three levels of flow rate is the minimum number we could use to get a measure of the non-linearity of the flow rate effect. Two fluid types were chosen: water and a 50% solution of propylene glycol (PG). Due to the limited range of tilt angles possible within the confines of the solar simulator, only two tilt angles (60 and 90 degrees from horizontal) were chosen for the tests.

Twelve tests were defined: six using water as the heat transfer fluid, and six using a 50% solution of PG and water. The order that the tests were performed was randomized within each group of six tests with the same heat transfer fluid, to reduce any unintentional correlation between successive tests. The order that the tests were performed in is the alphabetical order of the tests listed in the right-most column of Table 2.1.

The six tests that were done with 50% PG as the heat transfer fluid were all done with a collector tilt angle of 60 degrees from horizontal. Three of those tests were done with volume flow rates equal to the volume flow rate that were used for the tests with water as the heat transfer fluid, and the other three tests were done with the same product of mass flow rate and fluid thermal capacitance (m•Cp) as the

corresponding tests with water. This was done so that we could more directly evaluate the effect of using different fluids, independent of the capacity of the fluid to carry heat out of the collector.

The majority of the collector test was carried out at four different inlet temperatures of 25 °C, 45 °C, 65 °C and 85 °C. For the tests carried out at the lowest flow rate of 0.01 kg•s^{-1}, the highest inlet temperature we used was 80 °C so that the fluid outlet temperature would stay below 100 °C. At each of the four inlet temperature conditions, four periods of five-minute data were collected and averaged to provide a total of 16 data points from which to calculate a collector efficiency equation for the collector.

Both linear and nonlinear efficiency curve coefficients were calculated from the raw measurements. An example of the test data for the highest water flow rate is printed on the following page. The efficiency coefficients were based on a gross collector area of 2.869 m^2 and a reduced temperature difference (ΔT^*) based on mean collector temperature.

$$\Delta T^* = (Tm - Ta) / G$$

Tm = average of heat transfer fluid inlet and outlet temperature (°C)
Ta = ambient air temperature (°C)
G   = Solar irradiance on the aperture of the solar collector (W/m^2)

Thermal Efficiency Test Data
NRCan / Enerworks

Date/Time	Len min.	G W/m²	Gdn W/m²	Ta °C	Ti °C	ΔT °C	Ws m/s	ṁ·Cp W/°C	ṁ* kg/s	Ti-Ta °C	(Ti-Ta)/G °C m²/ W	η	ΔP kPa
2012-04-19 12:24	5	811	n/a	25.1	25.0	7.15	3.9	239.5	0.0573	-0.1	-0.0001	0.736	n/a
2012-04-19 12:29	5	811		25.1	25.0	7.13	3.9	239.4	0.0573	-0.1	-0.0001	0.734	
2012-04-19 12:34	5	810		25.1	25.0	7.14	3.9	239.7	0.0574	-0.1	-0.0001	0.736	
2012-04-19 12:40	5	811		25.1	25.0	7.14	3.9	239.6	0.0573	-0.1	-0.0001	0.736	
2012-04-19 13:35	5	807		25.0	45.0	6.22	3.9	239.2	0.0572	20.0	0.0248	0.643	n/a
2012-04-19 13:55	5	807		25.1	45.0	6.23	3.9	239.1	0.0572	19.9	0.0247	0.643	
2012-04-19 14:00	5	808		25.1	45.0	6.23	3.9	239.2	0.0572	19.9	0.0247	0.643	
2012-04-19 14:05	5	806		25.0	45.0	6.22	3.9	239.1	0.0572	20.0	0.0248	0.643	
2012-04-19 15:14	5	810		25.0	65.0	5.28	3.9	238.3	0.0570	40.0	0.0494	0.541	n/a
2012-04-19 15:19	5	809		25.0	65.0	5.29	3.9	238.1	0.0570	40.0	0.0494	0.543	
2012-04-19 15:24	5	807		25.1	65.0	5.26	3.9	238.3	0.0570	40.0	0.0495	0.541	
2012-04-19 15:29	5	808		25.0	65.0	5.27	3.9	238.2	0.0570	40.0	0.0495	0.542	
2012-04-20 8:43	5	809		25.0	85.0	4.19	3.9	236.8	0.0567	60.0	0.0742	0.428	n/a
2012-04-20 8:48	5	809		25.0	85.0	4.20	3.9	236.6	0.0566	60.0	0.0742	0.428	
2012-04-20 8:53	5	811		25.0	85.0	4.20	3.9	237.0	0.0567	60.0	0.0740	0.428	
2012-04-20 8:58	5	810		25.1	85.0	4.20	3.9	236.8	0.0567	59.9	0.0740	0.428	

* mass flow rate is calculated from measured values of m•Cp.

Indoor Simulator Test
Direct Radiation Only

Test 'A'

|	
Collector Tilt:	**60⁰** from horizontal
Exova Sample No.:	**12-06-S0007-1**
Collector Model:	**COL-4X8-NL-SGI-SH10**
Test Date(s):	2012-Apr-19
Test Fluid:	**Water**
Mass Flow Rate:	0.057 *kg/s*
Wind Speed (average):	3.9 *m/s*
Gross Area:	2.869 *m²*
Aperture Area:	2.717 *m²*
Mean Ambient Temp.:	25.0 *℃*
Irradiance Intensity:	809 *W/m²*
Orientation:	Portrait

Curve Fits:

1st Order (SI units):

Eff = 0.740 - 4.139(Ti-Ta)/G

2nd Order (SI units):

Eff = 0.735 - 3.472(Ti-Ta)/G - 0.0111(Ti-Ta)²/G
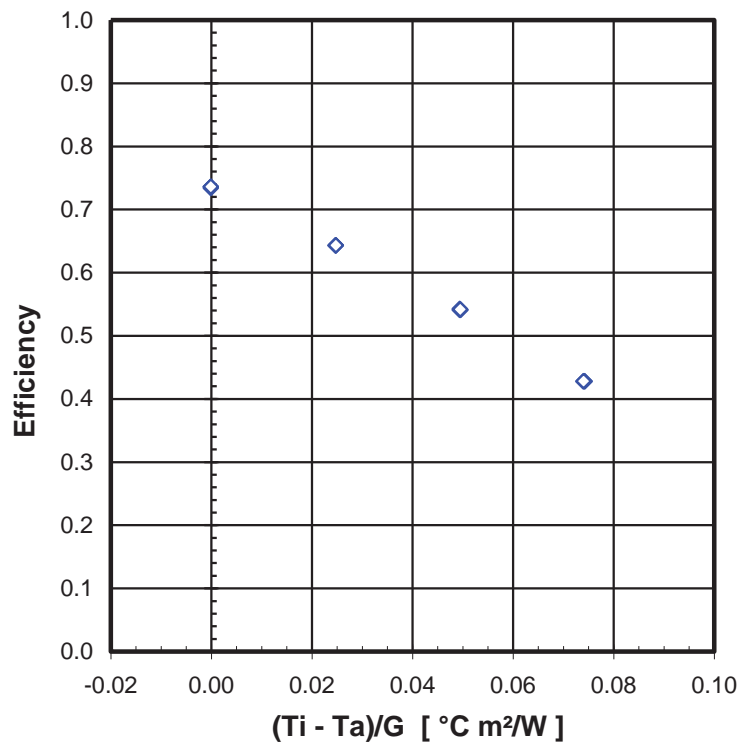
2.3 Collector efficiency for different volume flow rates

In the Drake Landing Solar Community (DLSC) project, the flow rate varied between 5% and 35% of the commonly-applied standard collector test flow rate of 0.02 kg•s^{-1}•m^{-2}. The lowest flow rates are used at DLSC when the solar irradiance is low and the inlet temperature to the solar collector array is high. In our study, we were not able to use as low a flow rate as used at DLSC, because of the requirement in our study to keep the solar irradiance constant at 800 W/m^2. Figure 2.2 shows how the fluid temperature rise in the collector varies with flow rate. To keep the fluid in the test collector below boiling temperature, while still allowing a workable range of inlet fluid temperatures, we chose total mass flow rates of water between 0.01 kg•s^{-1} and 0.057 kg•s^{-1} for our tests. This flow rate range covers the upper half of the flow rate range used at DLSC, and extends upward to include the commonly used standard test flow rate of 0.02 kg•s^{-1}•m^{-2}.
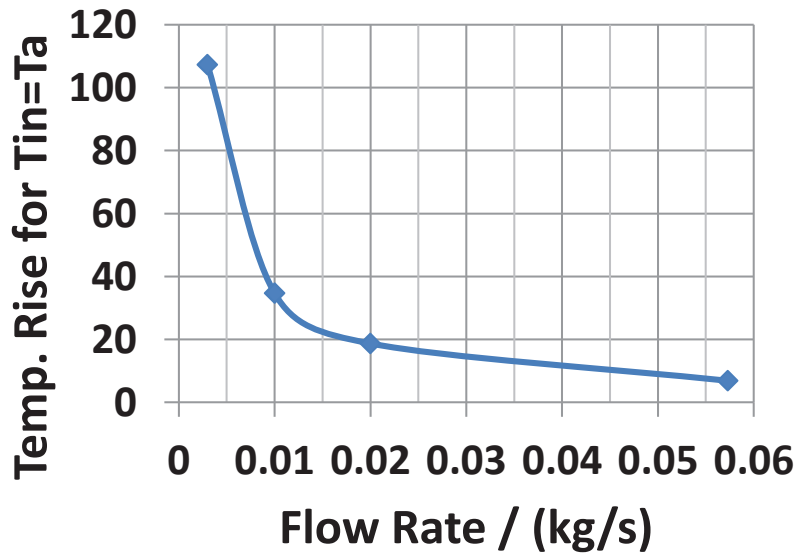

Figure 2.2: Predicted collector fluid temperature rise for various flow rates.

Fluid flow rate is commonly considered in North America to be the variable most influential on the efficiency of a liquid-heating glazed collector. This is because the North American convention is to describe collector efficiency as a function of reduced temperature based on inlet fluid temperature rather than mean fluid temperature. That is,

$\Delta T^{**} = (T_i - T_a) / G,$ rather than $\Delta T^{*} = (T_m - T_a) / G.$

Indeed, when efficiency is based on ΔT^{**}, the intercept efficiency increases an average of 12% over the 5.7 fold increase in water flow rate considered in this study, and the collector heat loss coefficient increases by 11%. In contrast, when the efficiency is based on ΔT^{*}, the dependence of the heat loss

coefficient on water flow rate becomes negligible (-0.4%), and the dependence of intercept efficiency on water flow rate is reduced to less than 2%.

The slope and intercept of the linear efficiency curves using water as the heat transfer fluid are plotted in Figure 2.3 to visually show the effect of varying the collector fluid flow rate. When collector efficiency is related to mean fluid temperature, it is apparent that there is a negligible effect on both intercept efficiency and heat loss coefficient.
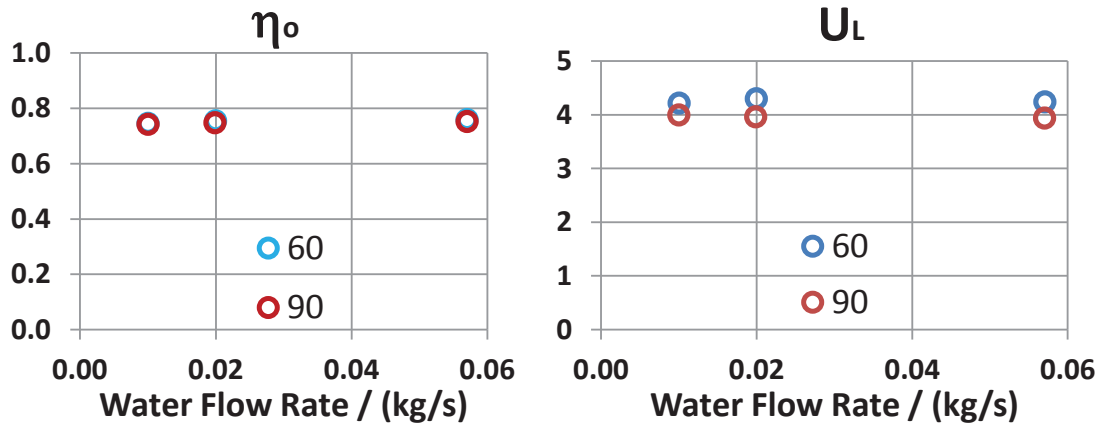

Figure 2.3: Collector efficiency linear coefficients for various test flow rates of water. Red circles are for the vertical collector and blue circles are for the collector at 60° tilt.

The result is somewhat different when 50% PG is used as the heat transfer fluid. These results are plotted in Figure 2.4, and they show an increase in collector efficiency with increase in fluid flow rate. The intercept efficiency increases an average of 5.8% and the heat loss term increases by 3.6%. This may be attributable to Reynolds number effects, as is discussed below in section 2.5.
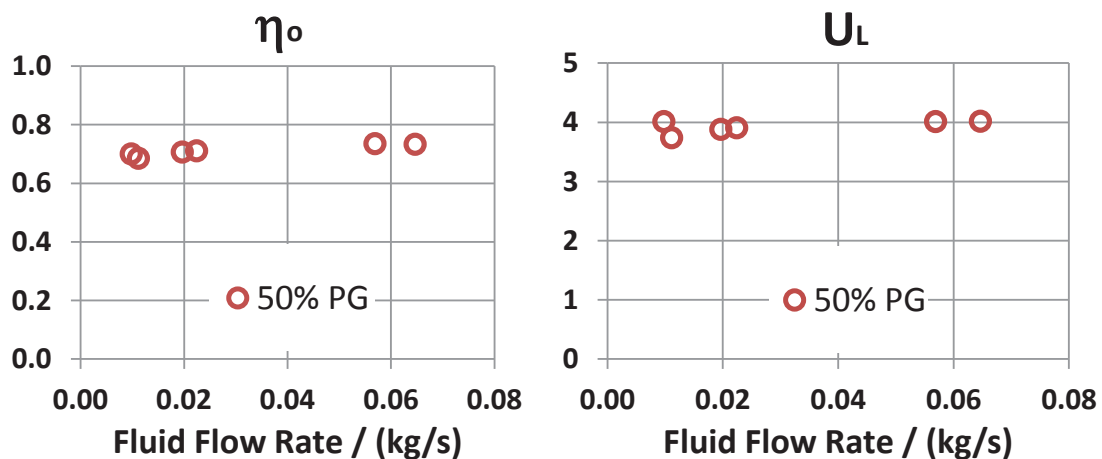

Figure 2.4: Collector efficiency linear coefficients for various test flow rates of 50% PG. All data are for the collector at 60° tilt.

2.4 Collector efficiency for different collector tilts

The slope and intercept of the linear efficiency curves for the six tests with water as the heat transfer fluid are plotted in Figure 2.5 as a function of tilt angle. These test results show that tilt angle only affects the heat loss coefficient, which decreases with tilt angle from horizontal by 7% on average over the limited range of these tests. The intercept efficiency decreases slightly—only 0.7% on average, which is likely comparable to the repeatability of the measurements.

It is to be expected that the collector heat loss from the glazing would be less for the vertical collector than for the collector tilted at 60 degrees, because the convective heat transfer between the cool glazing and the hot absorber plate will be less in a vertical air space. However, as mentioned above in section 2.2, the collector in the vertical orientation was tested at a lower average wind speed over its aperture. The observed reduction in heat loss from the collector may therefore be attributed to both lower internal and external convective heat transfer. Detailed modeling of the top heat loss from the collector, including estimates of both the internal and external convection heat transfer, would be required to separate the observed effect into an effect of wind speed and an effect of tilt angle.
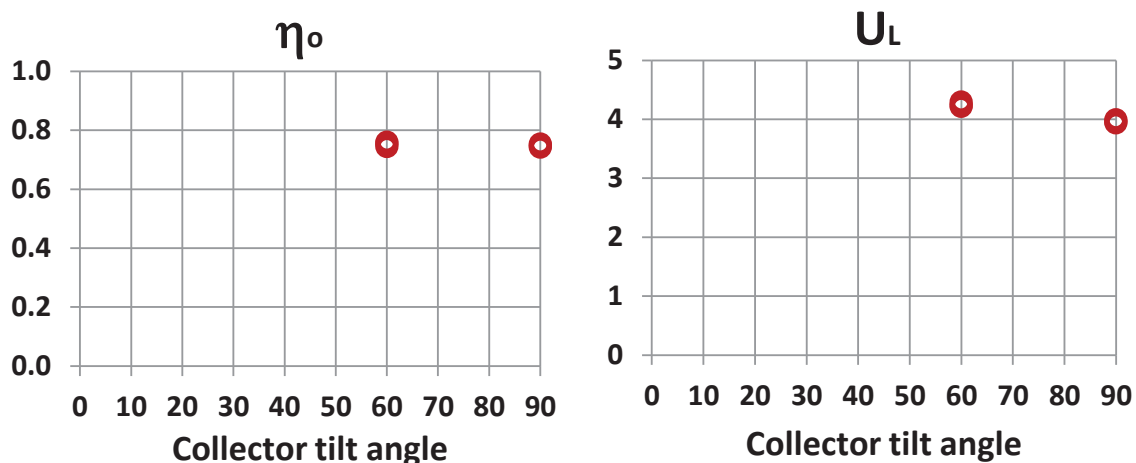

Figure 2.5: Collector efficiency linear coefficients for two different tilt angles.

2.5 Collector efficiency for different solar collector fluids

Three of the tests with 50% propylene glycol (PG) as the heat transfer fluid were performed with mass flow rates equal to the mass flow rates used in the tests with water. The other three tests with 50% PG were performed with higher flow rates, so that the product of mass flow rate times fluid thermal capacitance (m•Cp) was the same as for the tests with water. In this way, we attempted to separate the effect of the heat carrying capacity of the fluid from other effects. The results are plotted in Figure 2.6.
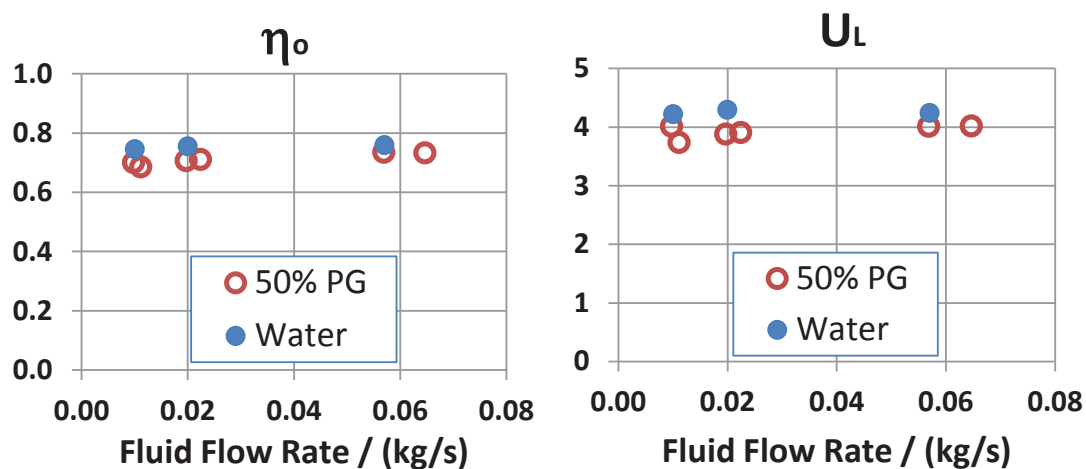
Figure 2.6: Comparison of collector efficiency linear coefficients for two different heat transfer fluids and for a range of test flow rates.

The obvious effect of using 50% PG is that the performance of the collector is reduced compared to using water as the heat transfer fluid. That result holds whether the mass flow rate is held constant or whether the product of (m•Cp) is held constant. When (m•Cp) is the same between the tests, the average intercept efficiency is 5.3% lower, and the heat loss coefficient is 6.9% lower with PG than with water. When the mass flow rate is the same between the tests, the average intercept efficiency is 5.9% lower, and the heat loss coefficient is 9.0% lower with PG than with water. The larger difference between fluid types suggested by these tests is mostly attributable to the one test with the lowest flow rate of PG. That one test resulted in lower collector performance than would be suggested by the trends of the other tests.

Taken all together, the results indicate that it is not just the fluid Cp that causes the difference between the performance of the two fluids, but perhaps other effects such as the difference in viscosity, which would have Reynolds number effects on the internal convection heat transfer coefficients.

We observed that the scatter (repeatability) in the test results is higher at low flow rates with 50% PG than it is with water. We can speculate that the increased variability is due to the sensitivity of the PG solution to Reynolds number effects, due to the higher viscosity of PG compared to water. The forced convection heat transfer coefficient on the inside of the fluid channels in the collector will be more sensitive to viscosity at the lower flow rates, where the Reynolds number is closer to the transition between laminar and turbulent flow.

2.6 Summary of test results

The full range of all the test results is shown in the efficiency curve plots in Figure 2.7.
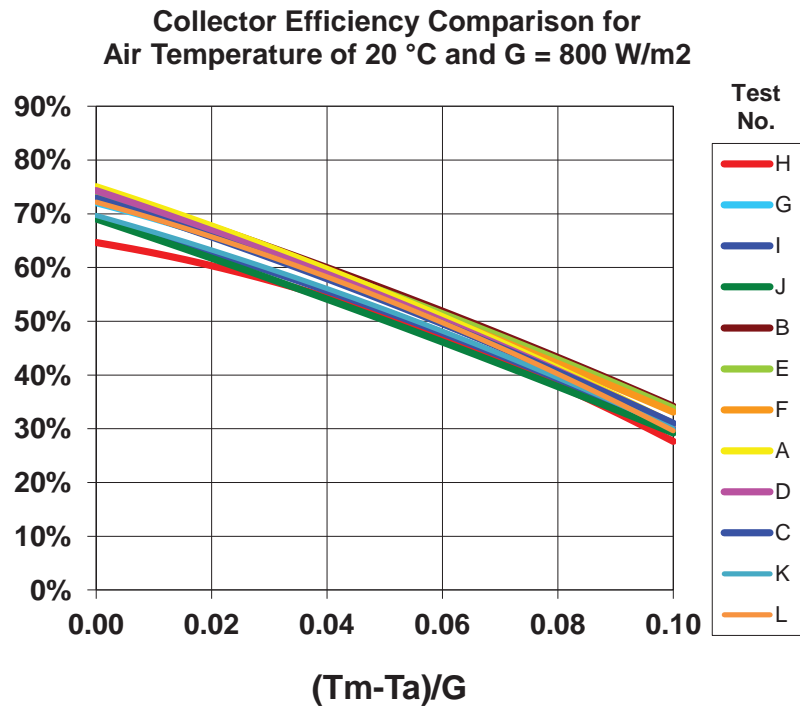

Figure 2.7: Measured collector efficiency curves for all tests combined.

Taking the linear efficiency equations as the basis for comparison, the full range of intercept efficiency is 22% of the mean, and the full range of heat loss coefficients is 25% of the mean. This is broken down into the separate effects of fluid type, collector tilt angle and heat transfer fluid flow rate in Table 2.2.

Table 2.2: Magnitude of effects of fluid type, tilt angle and flow rate on collector performance for the range of parameter variations in this study.

Parameter	Effect on η_o	Effect on U_L
Fluid Type	5.9% when (m•Cp) is constant 5.3% when mass flow is constant	9.0% when (m•Cp) is constant 6.9% when mass flow is constant
Collector Tilt	0.7%	7%
Mass Flow Rate	1.7% for water 5.8% for 50% PG	0.4% for water 3.6% for 50% PG

The analysis of the test results has shown that the largest effect is due to type of heat transfer fluid used, followed by tilt angle. When collector efficiency is expressed as a function of reduced temperature based on mean fluid temperature, the effect of fluid flow rate is small, except where a change in flow rate would cause a transition from laminar to turbulent flow in the fluid passages of the collector.

The details of the linear and second order fits to the data for all of the tests in this study are listed in Table 2.3.

Table 2.3: Summary of all test results.

Test ID	Test Fluid	Flow Rate (L/min per collector)	Flow Rate (Kg/s per collector)	Tilt Angle	Linear Eqn.		2nd Order Eqn.		
					η_o*	a_1*	η_o	a_1	a_2
C	Water	0.62	0.0101	60	0.745	4.220	0.729	3.450	0.0092
D	Water	1.22	0.0200	60	0.755	4.296	0.743	3.583	0.0095
A	Water	3.48	0.0571	60	0.759	4.242	0.750	3.457	0.0120
F	Water	0.61	0.0100	90	0.742	3.995	0.727	3.263	0.0087
E	Water	1.21	0.0199	90	0.748	3.961	0.738	3.339	0.0082
B	Water	3.48	0.0571	90	0.753	3.939	0.747	3.429	0.0078
J	50% PG	0.58	0.0098	60	0.700	4.013	0.691	3.569	0.0052
I	50% PG	1.16	0.0197	60	0.706	3.879	0.692	3.006	0.0114
G	50% PG	3.34	0.0569	60	0.735	4.012	0.721	2.801	0.0183
H	50% PG	0.66	0.0112	60	0.686	3.736	0.647	1.777	0.0240
K	50% PG	1.32	0.0224	60	0.711	3.903	0.697	3.025	0.0118
L	50% PG	3.79	0.0647	60	0.733	4.019	0.722	2.964	0.0161

Chapter 3: Danish investigations

3.1 Description of the investigated solar collector

The two investigated solar collectors were the models HT-SA 35-10 and HT-A 35-10, manufactured by the Danish company ARCON Solar A/S. These are large scale solar collectors and are normally used in solar collector fields for district heating application in Denmark.

The collectors were largely identical in terms of design and technical specifications and the only relevant difference was a 0.025 mm thick FEP (Fluorinated Ethylene Propylene) foil. The different appearance of the two collectors can be seen in Figure 3.1.

Figure 3.1: Solar collector HT-A 35-10 (left) and HT-SA 35-10 (right) at the Department of Civil Engineering at the Technical University of Denmark.

The collectors were installed beside each other, so that they experienced identical weather conditions. They both had an orientation of 9.5° West with respect to South, while the tilt angle could be changed through the use of semi-mobile scaffolding. Both collectors had external dimensions of 2.27 x 5.96 x 0.14 m with a total gross area of 13.57 m^2, while the aperture area was equal to 12.56 m^2. The absorber consisted of 18 aluminium strips covered by a selective coating. Each collector had two manifolds with a diameter of 35 mm, placed vertically along the sides and connected by 18 horizontal copper tubes with a diameter of 10 mm, laser-welded below the absorber strips. The external cover was made of an anti-reflective treated glass with a thickness of 3.2 mm. The insulation consisted of mineral wool, with a thickness of 75 mm below and 30 mm along the edges.

3.2 Test facility and test conditions

The solar collectors were installed and tested outdoors, in a solar collector test facility at the Technical University of Denmark. The fluid flow rates to the collectors were measured by two electromagnetic flow meters manufactured by Kamstrup (model MP240 and MP115 for the collector HT-A and HT-SA respectively) with an accuracy of 1.5%. The inlet temperatures were measured by type TT thermocouples using a copper-constantan junction, while the temperature differences between outlet and inlet temperature were measured by thermopiles with five copper-constantan junctions at each measuring point. The total radiation on the collector plane was measured independently for each collector by a CM11 pyranometer, produced by Kipp & Zonen and fulfilling the requirements of the highest accuracy class according to the norm ISO 9060. The diffuse radiation was measured by a similar pyranometer equipped with a shadow band.

The collectors were tested with a tilt angle of 45° at 5, 10 and 25 litres min^{-1} between 2011 and 2012, and then with tilt angles of 30° and 60° at 25 litres min^{-1} in 2013, using a propylene glycol/water mixture with a 40% weight concentration as solar collector fluid. Due to damages suffered during wind storms in autumn 2013, the solar collector HT-A became unusable. Hence, the later tests were carried out in the spring and summer 2014 on the original HT-SA collector only, for a tilt angle of 45°, a flow rate of 25 litres min^{-1} and using pure water as solar collector fluid. After completing the measurements on the HT-SA collector, this was opened and its FEP foil removed, in order to make it like a HT-A collector and test it under the same operating conditions.

The collector efficiency expressions were evaluated according to the standard norm EN 12975-2, so at least four independent data points were obtained for at least four different temperature levels, in a range between 20 °C and 100 °C. These data points were then interpolated by means of regression according to the method of least squares and the collector efficiency was expressed by the equation:

$$\eta = \eta_0 - a_1 \cdot \frac{(T_m - T_a)}{G} - a_2 \cdot \frac{(T_m - T_a)^2}{G}$$

where η [-] is the collector efficiency, based on the aperture area of the collector,

η_0 [-] is the zero-loss efficiency,

a_1 [W m^{-2} K^{-1}] is the first order heat loss coefficient,

a_2 [W m^{-2} K^{-2}] is the second order heat loss coefficient,

T_m [°C] is the mean fluid temperature within the solar collector,

T_a [°C] is the ambient temperature,

G [W m^{-2}] is the total solar irradiance on the collector plane.

Nevertheless, in case the second order heat loss coefficient a_2 is negative, the EN norm states that the efficiency expression must be computed in a first order form:

$$\eta = \eta_0 - a_1 \cdot \frac{(T_m - T_a)}{G}$$

The coefficients of the efficiency expressions for the different operating conditions are listed in Table 3.2 in section 3.8.

Also the incidence angle modifier (IAM) was evaluated according to the test procedure suggested in the norm EN 12975-2, but the tangent formula (Eq. 3.1) was used in place of the cosine formula, as the former proved to fit the experimental data more accurately than the latter.

$$IAM = 1 - \tan^p\left(\frac{\Theta}{2}\right) \qquad \text{(Eq. 3.1)}$$

where Θ [°] is the angle of incidence,

p [-] is the characteristic coefficient.

3.3 Influence of the FEP foil on the collector efficiency

As can be noted from the experimental values zero-loss efficiency (Table 3.2 in section 3.8) and Figures 3.2, 3.3 and 3.4, the presence of the FEP foil negatively affected the transmittance of the collector cover, causing a decrease in the zero-loss efficiency. On the other hand, neither the tilt angle nor the fluid flow rate had a major influence on the zero-loss efficiency. So, when supplied with a relatively cold fluid, the HT-A collector performed better than the HT-SA model. However, as the heat losses were lower in the HT-SA collector, the efficiency difference between the two models decreased with increasing mean temperatures until it became null for a certain value of reduced mean temperature. At this stage, any further increase in temperature entailed a better performance of the HT-SA collector with respect to the HT-A. As the fluid temperature generally increases from relatively low (~40 °C) to relatively high values (~85 °C) along a collector array in a solar heating field, a mixed composition of solar collectors with and without FEP foil seems to be the best solution, using collectors without foil in the first part of the array and collectors with foil in the second part, in order to optimally exploit their different characteristics.

3.4 Collector efficiencies for different volume flow rates

The two collectors were tested with propylene glycol/water mixture at different flow rates and constant tilt angle of 45°. The chosen flow rates were 5, 10 and 25 litres min^{-1}. The higher flow rate of 25 litres min^{-1} is in agreement with the recommendations prescribed by the standard EN 12975-2, which states that the fluid flow rate should be approximately 1.2 kg min^{-1} per unit aperture area of solar collector. In 2011, when these collectors were installed, collector rows in Danish solar heating field consisted of a lower number of collectors and 25 litres min^{-1} was the nominal flow rate in normal operating

conditions. Nevertheless, lower flow rates were used in the early morning and late afternoon, or generally whenever the solar irradiance was not sufficiently high, in order to be able to reach high return temperatures from the solar collector field. For this reason, flow rates of 5 and 10 litres min^{-1} were tested beside 25 litres min^{-1}.
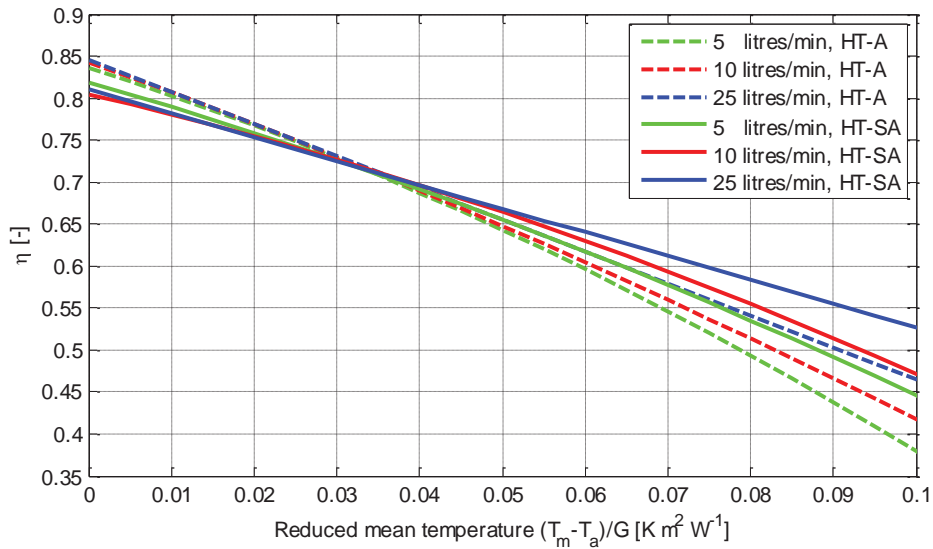

Figure 3.2: Efficiency curves for the HT collectors at different flow rates, 45° tilt and total solar irradiance G=1000 W m^{-2}.

As can be noted from the efficiency coefficients in Table 3.2 and seen in Figure 3.2, the efficiency expressions for 5 and 10 litres min^{-1} had the usual quadratic form, while those found for a flow rate of 25 litres min^{-1} were linear. Analysing the single efficiency data points (Figures 4.1 and 4.2 in section 4.2), it was found that the efficiencies measured at the highest temperature level were the main reason for the bending of the curves in the 5 and 10 litres min^{-1} cases, while efficiencies calculated at lower temperatures were largely aligned. This result was most likely due to the fact that heat losses in a solar collector increase more than linearly with the temperature difference between fluid and external environment, due to the radiation contribution (which becomes increasingly important at higher temperatures), the convection losses (which increase due to the lower viscosity of air between absorber and cover) and secondarily the conduction losses, as the thermal conductivity of mineral wool increases with temperature. Conversely, no bending appeared in the diagrams regarding 25 litres min^{-1} flow rate. The reason of this unexpected behaviour was found in the combination of high fluid velocity and low kinematic viscosity at the highest temperature level, resulting in large Reynolds numbers (Re≈3800-6300) and turbulent flow regime. This different flow regime led to a much higher heat transfer coefficient than laminar flow and hence was able to counteract the increased thermal losses. If measurements at higher temperature levels had been taken, a quadratic form of the efficiency expression would most likely have been found for 25 litres min^{-1} flow rate as well. Much attention should be paid when using these linear equations outside the temperature range for which they were

calculated, because extrapolation of the curves for higher values of the ratio $(T_m\text{-}T_a)/G$ would most likely overestimate the actual efficiency of the collectors.

3.5 Collector efficiencies for different collector tilt angles

The two collectors were also tested with propylene glycol/water mixture at different tilt angles, more specifically at 30°, 45° and 60°. The angles of 30° and 45° were chosen as they are respectively the lower and upper tilt angle usually adopted in solar collector fields in Denmark (Furbo et al., 2014). On the other hand, the angle of 60° was chosen as this is the tilt commonly used by test institutes when assessing the collector efficiency to be reported in the collector data sheet.
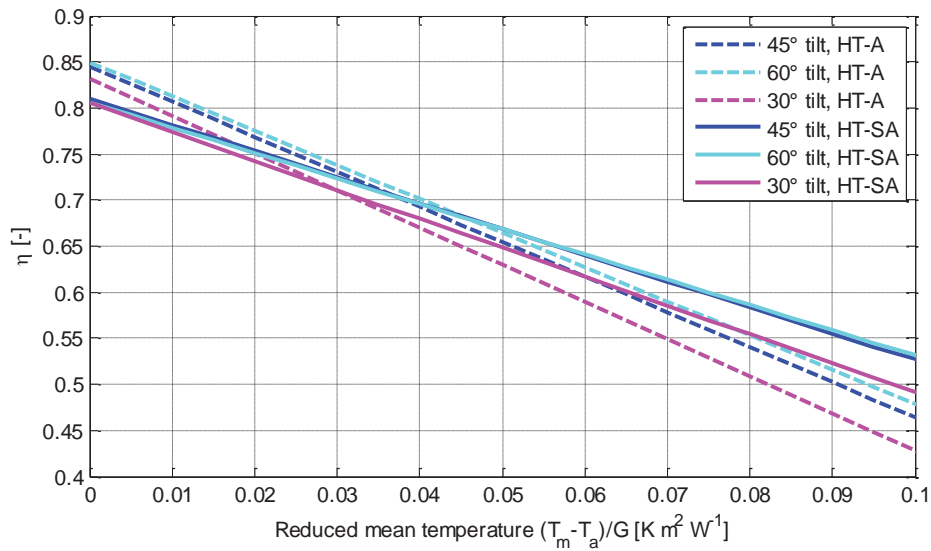

Figure 3.3: Efficiencies curves for the HT collectors at different tilt angles and 25 litres min^{-1}.

From Figure 3.3, it is seen that the larger the tilt angle, the higher the efficiency, due to the lower heat loss coefficient. The exact values of heat loss coefficients for the different tilt angles can be read in Table 3.2. From both Figure 3.3 and Table 3.2, it can be noted that the relation between tilt angle and efficiency was not linear for either of the collectors. In fact, taking 45° tilt as a reference, decreasing the angle to 30° (-33%) caused an increase in the first order heat loss coefficient by 6.3% and 10.6% for the collector HT-A and HT-SA respectively. On the other hand, a tilt of 60° (+33%) caused the same coefficient to decrease by only 2.4% and 3.2% for the collector HT-A and HT-SA respectively. In fact, in Figure 3.3 it is clear that the efficiency curves for the 45° and 60° tilt angles are very close to each other compared to those at 45° and 30° tilt.

This effect of the tilt angle on the heat losses is in agreement with theory, as both radiation and convection losses are expected to decrease when tilting a flat plate collector. In fact, when a collector is tilted, the view factor of the aperture area toward the earth surface increases, while the view factor

toward the sky is reduced. Since the radiation temperature of the sky is lower than that of the earth, a higher tilt positively affects the efficiency by reducing the radiation losses. Convective losses also decrease due to the reduced number of convective cells between the absorber and cover.

3.6 Collector efficiencies for different solar collector fluids

A mixture of propylene glycol and water is the most common fluid used in this kind of solar collectors, when they are installed in solar collector fields. Mixtures of propylene glycol and water have the advantage of being characterized by lower freezing temperatures and higher boiling points than pure water. So, they can successfully be used to avoid freezing of the fluid inside the collectors in winter and to reduce the risk of boiling and consequent stagnation. On the other hand, these mixtures present some drawbacks, such as lower specific heat per unit volume, higher viscosity (which negatively affects both the convective heat transfer coefficient and the pressure drop) and higher cost.

Although propylene glycol/water mixtures are used in solar collector fields, the collector efficiency stated in the technical data sheets usually refers to water as collector fluid. Given the better characteristics of water as collector fluid, it is of interest to know how much the fluid type influences the collector performance. For this reason, the two HT collectors were also tested using water as solar collector fluid, while supplied by a flow rate of 25 litres min^{-1} and tilted by 45°. The corresponding efficiency curves and the single efficiency data points can be seen in Figure 3.4. As comparison, the same figure also shows the efficiency data points obtained for a 25 litres min^{-1} flow rate of 40% glycol/water mixture and 45° tilt. A point-to-point comparison was preferred to a curve-to-curve comparison, because quadratic best fit curves obtained from efficiency points with different flow regime may be difficult to be compared properly.
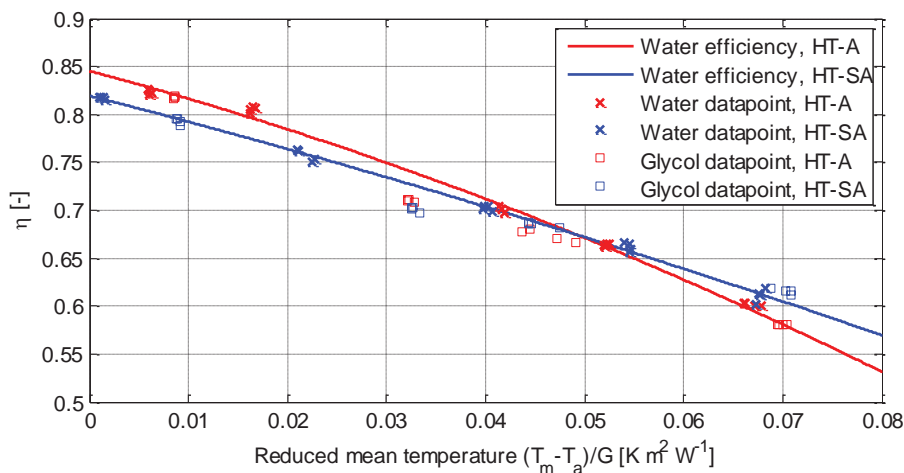

Figure 3.4: Efficiencies curves and efficiency data points (cross markers) using water in the HT collectors at 45° tilt angle and 25 litres min^{-1}. Square markers are the efficiency data points for glycol/water mixture at 45° tilt angle and 25 litres min^{-1}.

It can be seen that the efficiency points for water and for glycol/water mixture showed very similar trend when the fluid temperature was sufficiently low or sufficiently high, so that both fluids experienced the same flow regime. The relative difference in efficiencies in these circumstances is within the accuracy of the measurements.

For reduced mean temperature $(T_m-T_a)/G$ lower than 0.01 K m^2 W^{-1}, the flow of both glycol/water mixture and water in the absorber pipes was expected to be laminar. For higher values of reduced mean temperature, water flow in the collector pipes was turbulent, while a 40% glycol/water mixture was expected to experience fully turbulent regime only at high temperature, at least above 75 °C in case of a 25 litres min^{-1} flow rate. This combination of temperature of flow rate corresponds to a Reynolds number of approximately 3000 in the horizontal pipes of a HT 35-10 collector (if uniform flow distribution is assumed). Among the glycol/water efficiency points shown in Figure 3.4, the only ones which respected this temperature requirement were those with reduced mean temperature of approximately 0.067 K m^2 W^{-1} (cross markers in the bottom right corner of the figure), which corresponded to Re of about 4600.

Water/glycol efficiency points shown in the figure and having reduced mean temperatures between 0.04 and 0.05 K m^2 W^{-1} ($Re\approx2200$) appeared to have slightly lower efficiency values compared to water efficiency points obtained for similar temperature levels (reduced mean temperatures of about 0.04 and 0.053 K m^2 W^{-1}). This might be due to the fact that the glycol/water mixture in these conditions was already in transitional regime, and hence characterized by higher thermal heat transfer coefficient than purely laminar regime.

The difference in efficiency between water and glycol/water mixture was much more evident when the former was in turbulent regime and the latter in laminar regime, as can be seen for reduced mean temperatures between 0.015 and 0.04 K m^2 W^{-1} in Figure 3.4. The relative difference between glycol/water efficiency points and the water efficiency read from the curve was 4.3% and 3.4% for the collector HT-A and HT-SA respectively.

As a conclusion, water performed better than glycol/water mixture as was expected, but the key factor seemed to be the flow regime experienced by the fluid, which played a more important role than the difference in specific heat per unit volume, thermal conductivity and viscosity of the two fluids. As a quick way to assess whether the flow regime is laminar, transitional or turbulent, a flow regime map is shown in Figure 3.5.
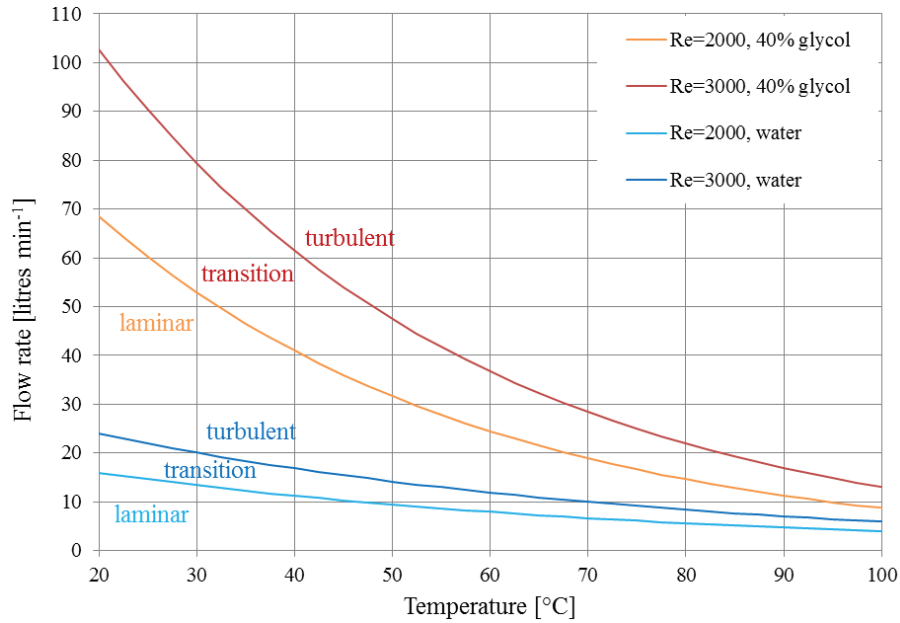
Figure 3.5: Flow regime map of a HT 35-10 collector for 40% glycol/water mixture and pure water, as function of fluid temperature and collector flow rate. Laminar regime is assumed for *Re* lower than 2000, while turbulent regime for *Re* higher than 3000.

Figure 3.5 shows the collector flow rates, as function of temperature, giving *Re*=2000 (transition from laminar to transitional flow) and *Re*=3000 (transition from transitional to turbulent flow) for both a 40% glycol/water mixture and pure water. The chart assumes that the collector flow rate is equally distributed in the 18 horizontal pipes of the absorber.

The *Re* values of 2000 and 3000 were chosen both because they are common values read in literature and because they were suggested from a series of pressure drop measurements carried out on the HT-SA collector in 2014. These tests were performed using a TA-SCOPE differential pressure sensor, manufactured by TA Hydronics and characterized by an accuracy given by the maximum value between 1% of the reading and 0.1 kPa. The collectors were supplied with water at a mean temperature between 20 °C and 30 °C, and varying the flow rate between 10 and 30 litres min^{-1}. As the pressure drop measurements were taken at the inlet and outlet of the collector, the contribution given by the inlet/outlet connections and manifolds needed to be estimated and subtracted, in order to identify the pressure drop due to the horizontal pipes only. The pressure drops given by inlet/outlet connections and manifolds were evaluated using correlations found in literature (Idelchik, 1994). When the pressure drop across the horizontal pipes was isolated, the Darcy friction factor was evaluated according to the following correlation:

$$f = \frac{2\,D \cdot \Delta p}{L \cdot \rho \cdot w^2}$$

where f [-] is the Darcy friction factor,

        D [m] is the inner diameter of the horizontal pipe,

        Δp [Pa] is the pressure drop across the horizontal pipe,

        L [m] is the length of the horizontal pipe,

        ρ [kg m^{-3}] is the fluid density evaluated at the mean fluid temperature across the collector,

        w [m s^{-1}] is the mean fluid velocity in the horizontal pipe.

The results of these tests are shown in Figure 3.6 in terms of Darcy friction factor as function of the Reynolds number.
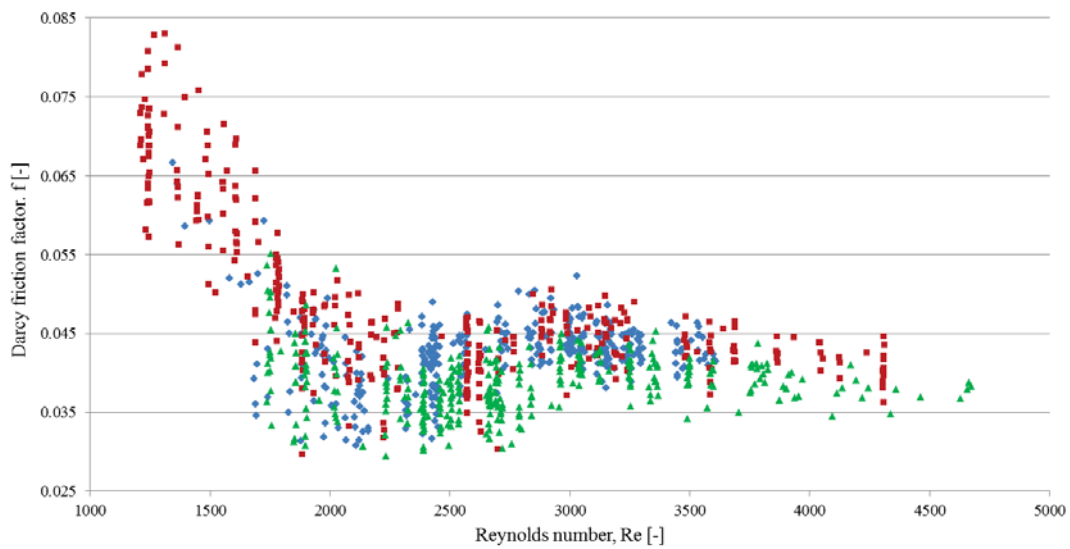

Figure 3.6: Darcy friction factor as function of the Reynolds number in the horizontal pipes of HT-SA 35-10 collector. Different markers denote different tests.

3.7 Incidence angle modifier

The IAM was measured in all the different operating conditions and the values of the p exponent are listed in Table 3.1. Despite the scattered values, characterized by similar standard deviation (0.12 and 0.10 for the collector HT-A and HT-SA respectively), the results showed clearly that the presence of the FEP foil reduced the optical properties of the cover, as the HT-A collector had a higher IAM curve than the HT-SA model in every operating condition. On the other hand, tilt angle and flow rate did not appear to influence the IAM in a specific way, so that if a single value of the p exponent needed to be chosen, the simplest approximation would consist in using the arithmetic mean, which is equal to 3.9 and 3.6 for the solar collector HT-A and HT-SA respectively.

Table 3.1: Exponent p in the tangent formula of the incidence angle modifier.

Tilt angle [°]	Flow rate [litres min^{-1}]	Fluid type	p exponent HT-A	p exponent HT-SA
45°	5	40% glycol	4.08	3.65
45°	10	40% glycol	3.73	3.37
45°	25	40% glycol	3.78	3.60
60°	25	40% glycol	3.96	3.65
30°	25	40% glycol	3.77	3.57
45°	25	water	3.80	3.67
Mean			3.85	3.58
Standard deviation			0.12	0.10

3.8 Summary of test results

A comprehensive and compact overview of the efficiency test results for all the tested operating conditions is given in Table 3.2. As explained in the previous sections, the effect of the presence of the FEP foil on the zero-loss efficiency and on the heat losses, the influence of the tilt angle, flow rate and fluid type on the efficiency parameters can here be assessed in a quantitative way.

Table 3.2: Summary of test results.

Collector model	Fluid type	Flow rate [litres min^{-1}]	Tilt [°]	η_0 [-]	a_1 [W m^{-2} K^{-1}]	a_2 [W m^{-2} K^{-2}]
HT-A	40% glycol	5	45	0.835	3.13	0.0143
HT-A	40% glycol	10	45	0.843	3.55	0.0070
HT-A	40% glycol	25	45	0.845	3.80	-
HT-A	40% glycol	25	60	0.850	3.71	-
HT-A	40% glycol	25	30	0.832	4.04	-
HT-A	water	25	45	0.845	2.75	0.0146
HT-SA	40% glycol	5	45	0.818	2.76	0.0096
HT-SA	40% glycol	10	45	0.804	2.26	0.0107
HT-SA	40% glycol	25	45	0.810	2.83	-
HT-SA	40% glycol	25	60	0.806	2.74	-
HT-SA	40% glycol	25	30	0.805	3.13	-
HT-SA	water	25	45	0.820	2.66	0.0057

Direct comparison of the efficiency curves can be done, when no change in flow regime occurs throughout the temperature range at which the collectors are tested: for example 5 and 10 litres min^{-1} flow rates in this study. On the other hand, when the flow regime switches from laminar to turbulent across the investigated temperature range, a change in the profile of the efficiency curve occurs and a

simple quadratic expression cannot interpolate the data accurately. In these cases the slope of the efficiency curve and secondarily the zero-loss efficiency are affected by the amount of points taken in the three different flow regime conditions and by the temperature level at which regime transition occurs. Consequently, much attention should be paid in drawing conclusions regarding the efficiency expression parameters, and a point-by-point analysis is more advisable. Alternatively, and in case enough measurement points are available, the efficiency points may be grouped according to different flow regime conditions and the regression done on each subgroup.

Chapter 4: Analyses on prediction methods to determine efficiencies for collectors in operation in solar collector fields

4.1 Simulation software for solar collector efficiency: *Soleff*

The calculation of the experimental efficiency curves is of key importance to assess the actual performance of the collectors under given operating conditions. It could be both interesting and useful to have a model able to evaluate the collector efficiency also under conditions that differ from those tested. Models of the two ARCON collectors were created using Soleff, a solar collector simulation software developed at Technical University of Denmark (Rasmussen and Svendsen, 1996).

Soleff requires a large number of input parameters, ranging from design characteristics of the collector to operating and weather conditions. Regarding the weather conditions, measured data were used whenever available. The earth radiation temperature and the sky temperature were assumed equal to the ambient temperature and to the ambient temperature decreased by 20 K respectively. Most of the collector characteristics were found either in the collector data sheets or in literature (Rasmussen and Svendsen, 1996; Furbo and Shah, 2003). Input parameters for which the exact value could not be found were assumed according to common values found in literature and iteratively modified in order to obtain the best fit with the experimental data.

Despite the large number of different aspects which is considered by Soleff, this software cannot take into account the complexity of the real-world operation. For example, the software assumes uniform flow distribution in the different pipes, constant fluid properties across the collector and sudden change from laminar to turbulent flow regime at a Reynolds number of approximately 2200. The last one proved to be the less accurate simplification, as measured efficiencies obtained for Reynolds numbers between 2200 and 2500 were always lower than those computed by the Soleff models (which assumes turbulent regime in this range) and pressure drop measurements showed transitional behaviour for Reynolds numbers between 2000 and 3000 (as seen in Figure 3.6). Then, increasing slightly the pipe diameter in the simulation models, the flow was forced to be laminar and the efficiency in this case was calculated. So, the experimental results could be compared to those returned by the simulation models, in both cases where turbulent and laminar flow was assumed.

4.2 Comparison between *Soleff* and experimental efficiencies

The simulation models developed in Soleff were used to evaluate the theoretical efficiency of the two collectors, based on the weather and operation conditions measured during the efficiency tests.

The measured and the theoretical efficiency points for propylene glycol/water mixture at the different flow rate and tilt angle conditions are shown in Figure 4.1 and Figure 4.2 for the solar collector HT-A and HT-SA respectively. For the sake of clarity, the efficiency points computed by the Soleff models at operating conditions corresponding to Reynolds numbers between 2200 and 2400 are not represented in Figure 4.1 and Figure 4.2, but are shown independently in Figure 4.3.
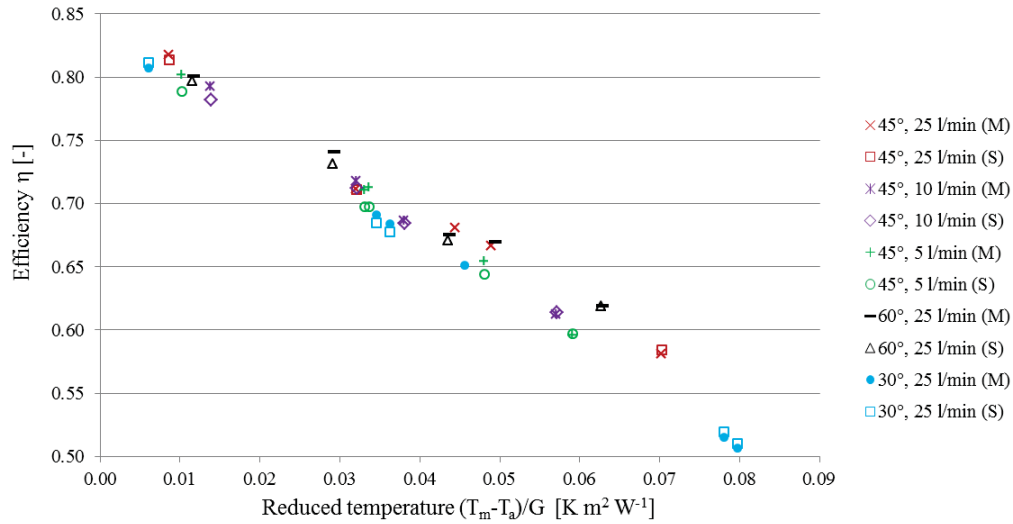

Figure 4.1: Comparison between measured (M) and simulated (S) efficiencies of the HT-A collector for glycol/water mixture at different tilts and flow rates.
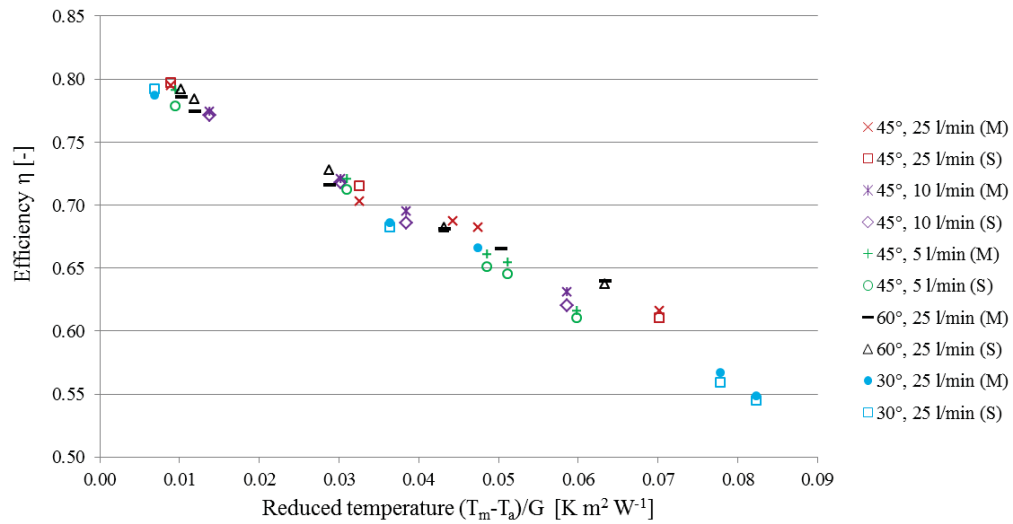

Figure 4.2: Comparison between measured (M) and simulated (S) efficiencies of the HT-SA collector for glycol/water mixture at different tilts and flow rates.

From Figure 4.1 and Figure 4.2 is noted that the simulation models fit the experimental data points in the laminar ($Re<2000$) and turbulent regime ($Re>3800$). The average relative difference between

experimental efficiency values and simulated ones is 1% for both the HT-A and HT-SA collector, while the maximum deviation is equal to 2.2% for the HT-A model and 1.8% for the HT-SA model. From the diagrams it is possible to notice that the experimental efficiency points at 5 and 10 litres min^{-1} are mainly aligned and then could be accurately interpolated by quadratic efficiency curves (see Table 3.2). On the other hand, efficiency points obtained for 25 litres min^{-1} flow rate presented some kind of discontinuity when the ratio $(T_m-T_a)/G$ was between 0.044 and 0.051 K m^2 W^{-1}. In fact the efficiency values for this temperature level were higher than what would be expected from the extrapolated curve fitting the efficiency points obtained for lower values of $(T_m-T_a)/G$.
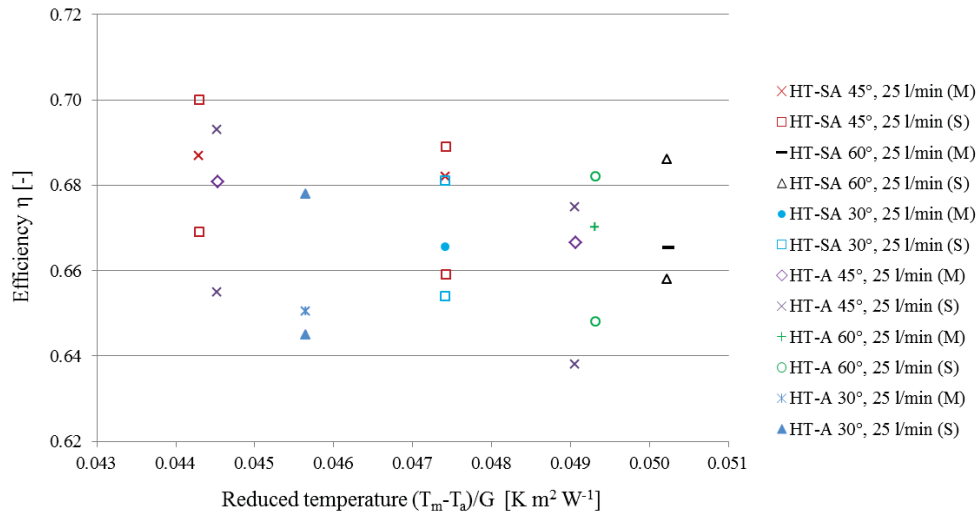

Figure 4.3: Comparison between measured (M) and simulated (S) efficiencies of HT-A and HT-SA collector for Reynolds numbers between 2200 and 2400. In each couple of simulated efficiency points the higher was obtained for turbulent flow and the lower was obtained forcing the Soleff models to assume laminar flow conditions.

In fact, the measured points with a value of the ratio $(T_m-T_a)/G$ between 0.044 and 0.051 K m^2 W^{-1} and 25 litres min^{-1} flow rate had Reynolds numbers between 2200 and 2400, which is usually considered to be characterized by transitional flow according to literature (Idelchik, 1994). These efficiency points showed intermediate characteristics between laminar and turbulent regime, both in terms of pressure drop (see Figure 3.6) and from the efficiency point of view (Figure 4.3). In fact, as can be seen in Figure 4.3, the efficiencies measured in this range of Reynolds number were always higher than those computed by the Soleff models for laminar flow, but lower than those obtained for turbulent flow. Nevertheless, no clear quantitative relation can be appreciated between the theoretical Reynolds number of the flow and the relative position of the experimental efficiency with respect to the two Soleff efficiency points. This means, for example, that an efficiency point characterized by a higher Reynolds number was not necessarily closer to the corresponding Soleff efficiency point obtained for turbulent flow. For example, if the HT-A collector is considered, the experimental efficiency point for

30° tilt (dark blue cross in Figure 4.3) is much closer to the corresponding Soleff efficiency in laminar conditions, than the efficiency points at 45° tilt (purple diamonds in the figure), although the former had $Re \approx 2400$, while the latter had $Re \approx 2200$. Transition from laminar to turbulent regime is a process which is not fully understood yet and fluid-dynamic properties of transitional flows are not simply functions of the Reynolds number, but are influenced by local irregularities and disturbances.

Similarly to previous figures referring to glycol/water mixture, Figure 4.4 shows the comparison between experimental and simulated efficiency points for water. The average relative difference between experimental efficiency values and simulated ones is 1% and 1.2% for the HT-A and HT-SA collector respectively, while the maximum deviation is equal to 1.5% for the HT-A model and 1.9% for the HT-SA model. These values are in agreement with those found for propylene glycol/water mixture.
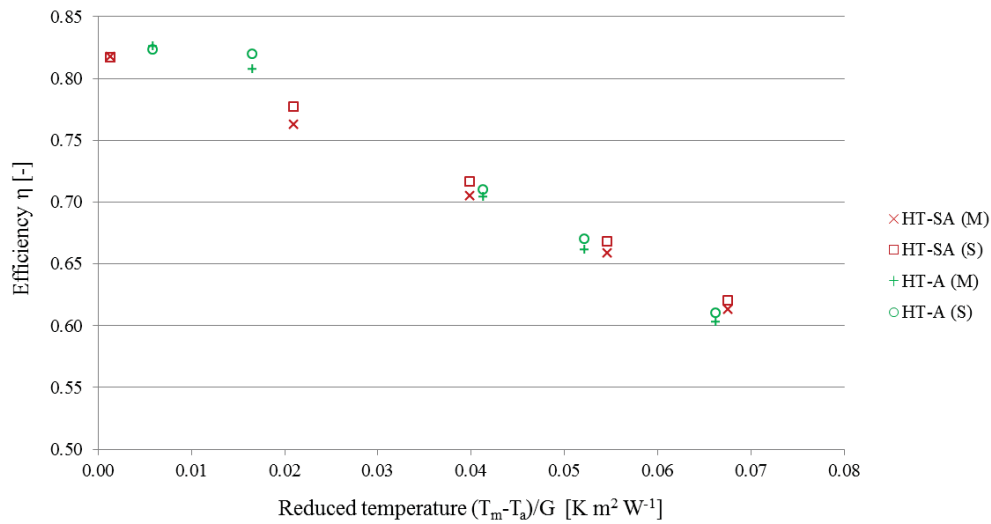

Figure 4.4: Comparison between measured (M) and simulated (S) efficiencies of both HT collectors for water at 45° tilt angle and 25 litres min^{-1} flow rate.

All the efficiency points with reduced mean temperature higher than 0.01 K m^2 W^{-1} are characterized by turbulent regime, while the points at the lowest temperature level appeared to experience laminar flow, which was suggested by the good agreement with Soleff results and the poor alignment with the other efficiency points, which are expected to be in turbulent conditions.

It should be noted that these efficiency points, which appeared to be in laminar conditions, were characterized by a Reynolds number of about 3500, so slightly higher than the value suggested by Figure 3.6 as transition from transitional to turbulent regime. The reason for this difference could be due to the fact that in the pressure loss tests, whose results are shown in Figure 3.6, the Reynolds number was varied manually changing the flow rate by means of a regulation valve. On the other hand, during the efficiency tests, the fluid was heated up to desired temperature level exploiting the solar radiation reaching the collector. As transition of flow regime is affected mainly by disturbances, it may be that the valve regulation caused the transition between laminar and turbulent regime to occur at lower Reynolds number than the gradual heating up of the fluid.

4.3 *Soleff* **efficiency expressions**

After that Soleff models had been calibrated on the experimental efficiencies, these could be used to estimate the efficiency curves of the two HT collectors in different operating conditions of flow rate, tilt angle and fluid type. The first conditions which were simulated were those experimentally tested. Later other combinations of flow rate, tilt angle and fluid type were used as well, in order to get a better understanding of the influence of the different parameters.

Soleff efficiency curves were obtained assuming 800 W m^{-2} as total solar irradiance on the collector plane, diffuse irradiance equal to 10% of the total solar irradiance, ambient temperature of 22 °C and wind speed of 2 m/s. The curves were obtained fitting single efficiency points with 10 K difference in mean fluid temperatures between each other. The analysed temperature range was between 22 °C and 102 °C. For glycol/water flow rates of 25 litres min^{-1}, Soleff models assumed transition between laminar to turbulent regime for a fluid temperature of 62 °C. Hence, Soleff laminar and turbulent expressions were obtained fitting efficiency points below and above this temperature respectively.

Table 4.1 and Table 4.2 list the efficiency coefficients returned by Soleff for different operating conditions of the two HT collectors. Flow rates are expressed both in terms of volume (litres min^{-1}) and mass flow rate (g s^{-1}), as the former is commonly used in data sheets and standards regarding solar collectors, while the latter is the input required by Soleff software.

Table 4.1: Efficiency coefficients from Soleff models for the HT-A collector.

Fluid type	Flow rate [litres min^{-1}]	Flow rate [g s^{-1}]	Flow regime	Tilt [°]	η_0 [-]	a_1 [W m^{-2} K^{-1}]	a_2 [W m^{-2} K^{-2}]
40% glycol	5	84.7	laminar	30	0.817	3.85	0.0051
40% glycol	5	84.7	laminar	45	0.820	3.77	0.0051
40% glycol	5	84.7	laminar	60	0.825	3.64	0.0050
40% glycol	10	169.4	laminar	30	0.823	3.87	0.0053
40% glycol	10	169.4	laminar	45	0.826	3.78	0.0053
40% glycol	10	169.4	laminar	60	0.831	3.65	0.0052
40% glycol	25	423.5	laminar	30	0.833	3.84	0.0066
40% glycol	25	423.5	turbulent	30	0.875	3.94	0.0066
40% glycol	25	423.5	laminar	45	0.837	3.76	0.0066
40% glycol	25	423.5	turbulent	45	0.877	3.84	0.0065
40% glycol	25	423.5	laminar	60	0.841	3.63	0.0064
40% glycol	25	423.5	turbulent	60	0.880	3.70	0.0064
40% glycol	45	765.0	turbulent	30	0.878	3.93	0.0070
40% glycol	45	765.0	turbulent	45	0.880	3.84	0.0069
40% glycol	45	765.0	turbulent	60	0.883	3.68	0.0069
water	25	410.0	turbulent	60	0.886	3.69	0.0070

Table 4.2: Efficiency coefficients from Soleff models for the HT-SA collector.

Fluid type	Flow rate [litres min^{-1}]	Flow rate [g s^{-1}]	Flow regime	Tilt [°]	η_0 [-]	a_1 [W m^{-2} K^{-1}]	a_2 [W m^{-2} K^{-2}]
40% glycol	5	84.7	laminar	30	0.801	3.22	0.0046
40% glycol	5	84.7	laminar	45	0.805	3.10	0.0048
40% glycol	5	84.7	laminar	60	0.809	2.94	0.0050
40% glycol	10	169.4	laminar	30	0.806	3.22	0.0047
40% glycol	10	169.4	laminar	45	0.810	3.10	0.0050
40% glycol	10	169.4	laminar	60	0.814	2.94	0.0051
40% glycol	25	423.5	laminar	30	0.814	3.18	0.0062
40% glycol	25	423.5	turbulent	30	0.849	3.31	0.0050
40% glycol	25	423.5	laminar	45	0.818	3.04	0.0069
40% glycol	25	423.5	turbulent	45	0.851	3.14	0.0055
40% glycol	25	423.5	laminar	60	0.822	2.92	0.0058
40% glycol	25	423.5	turbulent	60	0.856	3.02	0.0053
40% glycol	45	765.0	turbulent	30	0.850	3.24	0.0059
40% glycol	45	765.0	turbulent	45	0.853	3.13	0.0059
40% glycol	45	765.0	turbulent	60	0.854	2.89	0.0066
water	25	410.0	turbulent	60	0.856	2.91	0.0066

Figures 4.5 and 4.6 show some of the Soleff efficiency curves for the solar collectors HT-A and HT-SA respectively. For sake of clarity, the only curves shown are those referring to glycol/water mixture and flow rates up to 25 litres min^{-1}, so that it is possible to notice the strong effect of the transition from laminar to turbulent regime. According to the model, turbulent regime entails about 3 percent points higher efficiency compared to laminar flow.

Although Soleff assumes sudden change between fully laminar and fully turbulent conditions, this is not likely to happen in reality. As has been shown and explained in the section "Danish investigations", fluid flow does not switch from one regime to another at a precise value of Reynolds number, but transitional regime is experienced between laminar and turbulent conditions, showing intermediate characteristics between the two. Consequently, use of Soleff efficiencies for temperature level close to the transition region should be avoided.

It must be also noted that flow regime within the collector pipes is determined by the fluid temperature and not by the reduced mean temperature, as function of which the efficiency is expressed. This means that the value of reduced mean temperature at which transition occurs is not only function of the flow rate, but also of the solar irradiance and ambient temperature. Given the definition of reduced mean temperature (Eq. 4.1), this is about 0.05 K m^2 W^{-1} for 25 litres min^{-1} flow rate and 800 W m^{-2} irradiance, while it is higher for lower irradiances.

$$\text{reduced mean temperature} = \frac{T_m - T_a}{G} \quad \text{(Eq. 4.1)}$$

It may also be noted the positive effect of higher tilt angle and larger flow rate on the collector efficiency, as described in the previous section "Danish investigations".
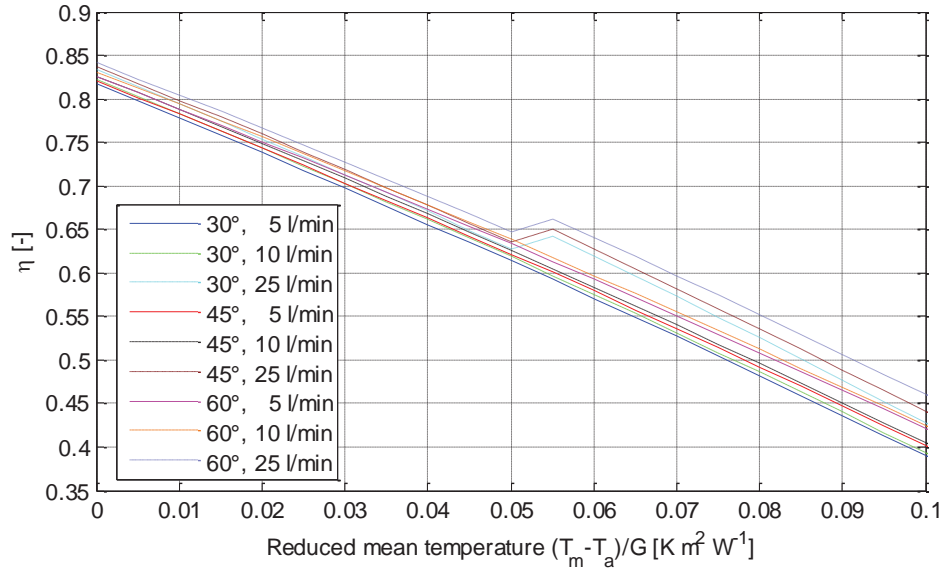
Figure 4.5: Soleff efficiency curves for the HT-A collector with 40% propylene glycol/water mixture and total solar irradiance G=800 W m^{-2} in different flow rate and tilt conditions.

Figure 4.6: Soleff efficiency curves for the HT-SA collector with 40% propylene glycol/water mixture and total solar irradiance G=800 W m^{-2} in different flow rate and tilt conditions.
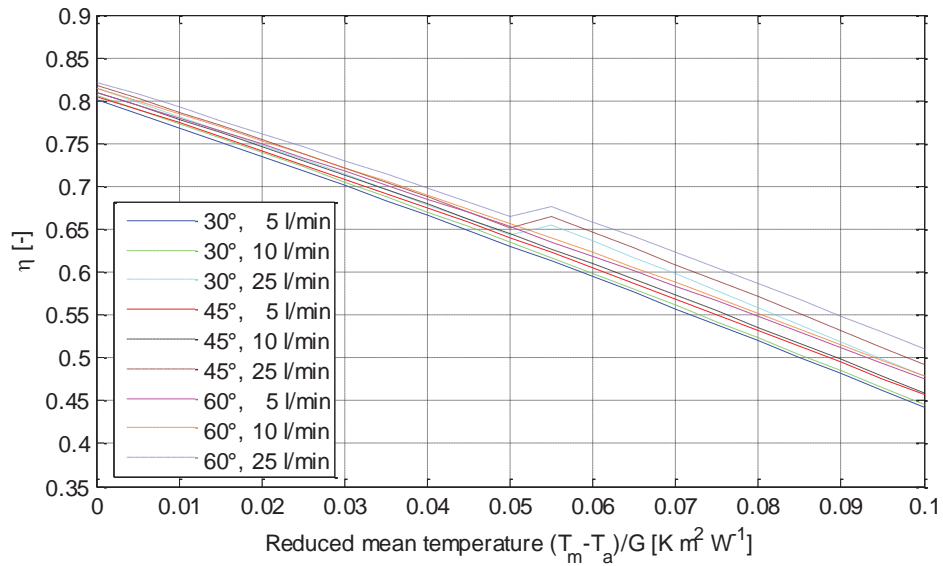
4.4 Overall efficiency expressions

Once the efficiency expressions for several tilt and flow rate conditions were known through Soleff simulation models, it was possible to write a unique efficiency formula which takes into account the dependence on these two different parameters. These formulas were developed for 40% propylene glycol/water mixture, as it is more relevant for real-world operation than water.

Purpose of this expression is the possible integration in simulation software for the assessment of the yearly heat production of solar collector fields, where especially the flow rate is likely to change during the year. In fact, many plants have a highly variable flow rate depending on the solar irradiance, in order to maintain a constant outlet temperature from the solar collector field. Another advantage is that these overall expressions can be used to estimate the collector efficiencies without need of installing Soleff software and knowing how to use it.

Due to the efficiency discontinuity caused by the transition in flow regime, two overall efficiency expressions were formulated for each collector, one for each of the two flow regimes considered by Soleff. The overall efficiency expressions in laminar condition were developed fitting data points calculated from the nine laminar efficiency curves listed in Table 4.1 and Table 4.2. The data points were chosen spaced by 0.01 K m^2 W^{-1}, in the range 0-0.10 K m^2 W^{-1} for 5 and 10 litres min^{-1} flow rate and 0-0.05 K m^2 W^{-1} for 25 litres min^{-1} flow rate, so that laminar regime was achieved. The overall expressions in turbulent condition were developed fitting data points calculated from the six turbulent efficiency curves for glycol/water mixture listed in Table 4.1 and Table 4.2. The data points were chosen spaced by 0.01 K m^2 W^{-1}, in the range 0.06-0.10 K m^2 W^{-1} for 25 litres min^{-1} flow rate and 0-0.10 K m^2 W^{-1} for 45 litres min^{-1} flow rate, so that turbulent regime was achieved. Data points for 45 litres min^{-1} were included in the regression in order to fit the overall expression also in a range of low reduced mean temperatures, for which the curves at 25 litres min^{-1} were not providing valid points.

Several expressions of this overall efficiency equation were formulated until the highest degree of correlation with Soleff efficiency curves was obtained. In order to evaluate the correlation between the overall efficiency equations and Soleff ones, the root mean square deviation (*RMSD*) was used. Given its definition (see Eq. 4.2), the *RMSD* represents the standard deviation of the differences between Soleff and overall efficiency data points.

$$RMSD = \sqrt{\frac{\sum_{i=1}^{N}\left(X_{all,i} - X_{Sol,i}\right)^2}{N}} \qquad \text{(Eq. 4.2)}$$

where *RMSD* [-] is the root mean square deviation,
$X_{all,i}$ [-] is the i-th efficiency value calculated through the overall efficiency expression,
$X_{Sol,i}$ [-] is the i-th efficiency value calculated through Soleff expression,
N [-] is the number of points used to evaluate the deviation.

When comparable degrees of correlation were found, the simplest expression was chosen.
The four overall efficiency expressions are reported below:

$$\eta_{HT\text{-}A,laminar} = \ [0.811 + 7.3 \cdot 10^{-4}\ F + 0.0228 \cdot (1\text{-cos}\beta)] +$$
$$- [4.029 - 0.0233\ F^{1/2} - 0.617 \cdot (1\text{-cos}\beta)] \cdot (T_m\text{-}T_a)/G +$$
$$- (0.0044 + 8.1 \cdot 10^{-5}\ F) \cdot (T_m\text{-}T_a)^2 \cdot G$$

$$\eta_{HT\text{-}A,turbulent} = [0.876 + 0.0137\cdot(1\text{-}\cos\beta)] +$$
$$- [4.254 - 0.00486\,F - 0.722\cdot(1\text{-}\cos\beta)]\cdot(T_m\text{-}T_a)/G +$$
$$- (0.0045 + 5.5\cdot10^{-5}\,F)\cdot(T_m\text{-}T_a)^2\cdot G$$

$$\eta_{HT\text{-}SA,laminar} = [0.796 + 5.8\cdot10^{-4}\,F + 0.0236\cdot(1\text{-}\cos\beta)] +$$
$$- [3.385 - 0.0268\,F^{1/2} - 0.689\cdot(1\text{-}\cos\beta)]\cdot(T_m\text{-}T_a)/G +$$
$$- (0.0042 + 6.5\cdot10^{-5}\,F)\cdot(T_m\text{-}T_a)^2\cdot G$$

$$\eta_{HT\text{-}SA,turbulent} = [0.848 + 0.0156\cdot(1\text{-}\cos\beta)] +$$
$$- [3.510 - 0.00427\,F - 0.750\cdot(1\text{-}\cos\beta)]\cdot(T_m\text{-}T_a)/G +$$
$$- (0.0040 + 4.9\cdot10^{-5}\,F)\cdot(T_m\text{-}T_a)^2\cdot G$$

where F [litres min^{-1}] is the flow rate,
β [°] is the tilt angle.

The *RMSD* values between the overall efficiency expressions and Soleff equations are listed in Table 4.3. The *RMSD* values were minimized for an irradiance of 800 W m^{-2}, for which Soleff curves were calculated. In Table 4.3 the deviations for 800 W m^{-2} are reported, as well as for 400 and 1000 W m^{-2}, which were assumed as lower and upper boundary respectively. Consequently, these irradiances were characterized by higher deviations. Intermediate irradiance values entail lower deviations.

Table 4.3: RMSD values between overall efficiency expressions and Soleff curves.

Irradiance [W m^{-2}]	Overall efficiency expression			
	HT-A laminar	HT-A turbulent	HT-SA laminar	HT-SA turbulent
400	$7.4\cdot10^{-4}$	$1.2\cdot10^{-3}$	$6.6\cdot10^{-4}$	$6.8\cdot10^{-4}$
800	$7.2\cdot10^{-4}$	$3.7\cdot10^{-4}$	$5.8\cdot10^{-4}$	$2.6\cdot10^{-4}$
1000	$7.8\cdot10^{-4}$	$6.5\cdot10^{-4}$	$6.7\cdot10^{-4}$	$4.7\cdot10^{-4}$

It can be noted that in all the overall expressions tilt angle influences the collector efficiency through the cosine function. This relation was chosen as it gave the best fit among all those tested and is in agreement with the relation between tilt angle and view factor from the collector to the sky (Eq. 4.3), which influences the radiation losses.

$$F_{coll\rightarrow sky} = \frac{1 + \cos\beta}{2} \qquad \text{(Eq. 4.3)}$$

where $F_{coll\rightarrow sky}$ [-] is the view factor from the collector to the sky.

The fit between overall expressions and Soleff points is reasonably accurate, as the values of *RMSD* are relatively low, with order of magnitude of 10^{-4}. The only exception is the HT-A collector in case of turbulent regime and 400 W m^{-2} irradiance, for which the *RMSD* is slightly higher (1.2 10^{-3}). The error introduced by the overall efficiency expressions is approximately 10 times smaller than that between experimental data points and Soleff models for fully laminar and turbulent conditions.

Chapter 5: Estimated yearly thermal performance of large scale solar collectors

5.1 Assumptions for yearly thermal performance evaluation

The thermal performance of a solar collector depends on the solar energy resource of the installation site. The key parameter describing the solar resource in a particular installation site is the solar radiation intensity per unit area. The amount of solar energy available varies between locations. Figure 5.1 shows the solar resource in different sites in Denmark according to the new Danish Design Reference Year (DRY), based on weather measurements recorded from 2001 and 2010 (DMI, 2012). The new DRYs replaced the previous Design Reference Year, which was valid for the entire country and based on the weather data from 1973 to 1989.
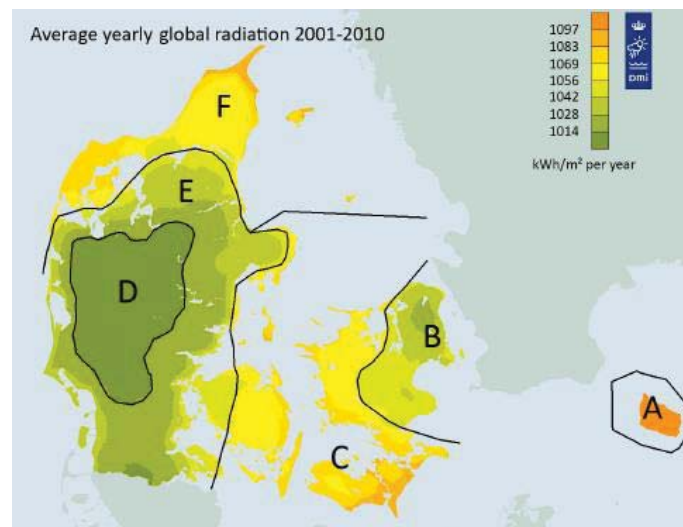
Figure 5.1: Yearly global radiation on a horizontal surface for the different radiation zones in Denmark (DMI, 2012).

The Danish DRY subdivides Denmark in 19 different zones by taking into account four key parameters: global radiation, outdoor temperature, wind velocity and air humidity. However, the most important parameter for the assessment of solar thermal performance is solar radiation, so that if only this parameter is considered the number of zones is reduced to six, which are shown in Figure 5.1.

When calculating the yearly thermal performance of the two different collectors, the mean fluid temperature and the flow rate were assumed constant throughout the year. The shadow effect from one

row to the following ones was considered, assuming a distance of 5 m between the rows (typical value in Danish solar collector fields) and a total number of rows of 30. Regarding the IAM, the average values of the *p*-exponent reported in Table 3.1 were used.

The yearly thermal performance so calculated was the energy collected by the solar collector fluid per unit collector area, and not that which could be actually utilized. In fact, no thermal loss occurring outside the solar collector was taken into account. In order to assess the actual useful energy, information about the losses which occur in the system connected to the collectors is required.

5.2 Results and discussion

First of all, the tilt angle giving the highest yearly thermal performance was investigated. In fact, lower tilt angles increase the radiation reaching the collector during the year and reduce the shadow effect, but they also entail poorer collector efficiency. The two radiation zones characterized by the highest and the lowest solar radiation throughout the year were chosen. These were zone A and zone D, which correspond to the island of Bornholm and the inner part of Jutland respectively, as seen in Figure 5.1. The optimum tilt angle was investigated in the specific case of a row distance of 5 m and a constant mean fluid temperature of 65 °C (turbulent flow regime) throughout the year. This temperature was chosen as mean fluid temperature within the solar collector field, as usually the inlet and the outlet temperature in Danish solar collector fields are about 45 °C and 85 °C respectively. The efficiency parameters were calculated using the appropriate overall efficiency expressions reported in section 4.4, assuming a constant flow rate of 25 litres min^{-1} and a tilt equal to the collector inclination angle.
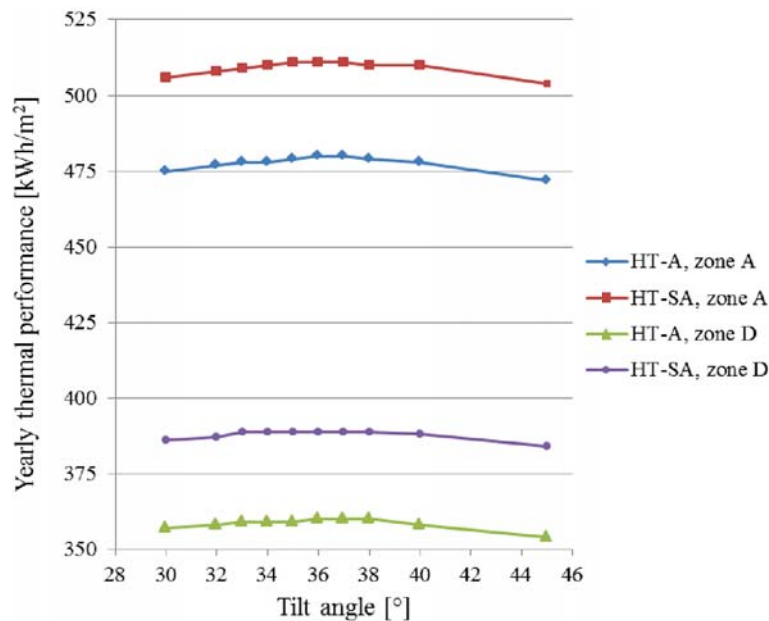

Figure 5.2: Yearly thermal performance for the HT collectors as function of the tilt angle for a fluid temperature of 65 °C in the radiation zones A and D.

Under these assumptions, the yearly thermal performance of the two collectors was found as function of the tilt angle and is shown graphically in Figure 5.2. It is seen that all curves present a quite flat maximum, which occurs for tilt angles between 35° and 38°. On the other hand, the yearly solar radiation on the collectors is maximized by lower tilt angles, in between 28° and 30° for both zone A and D, taking into account shadow effect between rows. This offset between the value of tilt angle maximizing the yearly thermal performance and that maximizing the yearly radiation is due to the fact that the collector efficiency is increasing with the tilt angle (see section 3.5). As the yearly thermal performance is influenced by both available solar radiation and collector efficiency, its maximum was found for a tilt angle which is slightly higher than the one maximizing the yearly solar radiation on the collector.

After choosing 36° as optimum tilt angle, the corresponding yearly thermal performance was computed. Figures 5.3 and 5.4 show the yearly energy output per unit collector area as function of the mean fluid temperature. In each diagram two yearly thermal performance curves are displayed. The first curve was obtained from an efficiency expression which refers to data sheet conditions, i.e. water as solar collector fluid, 25 litres min^{-1} flow rate and 60° tilt angle. Soleff efficiency expressions for water, reported in Tables 4.1 and 4.2, were used in this case. Such a case was taken into account because this is what is often done when planning solar collector fields: the data sheet efficiency of the collector is assumed, even if the collector array is tilted with a different angle and supplied with a different fluid type and fluid flow rate.

The second curve was calculated using an efficiency curve referring to more realistic conditions, such as 40% glycol/water mixture, a tilt angle equal to the actual collector tilt angle (36°) and 25 litres min^{-1} flow rate. At this purpose, the efficiency coefficients returned by the overall efficiency expressions with the proper tilt angle and flow rate were used.
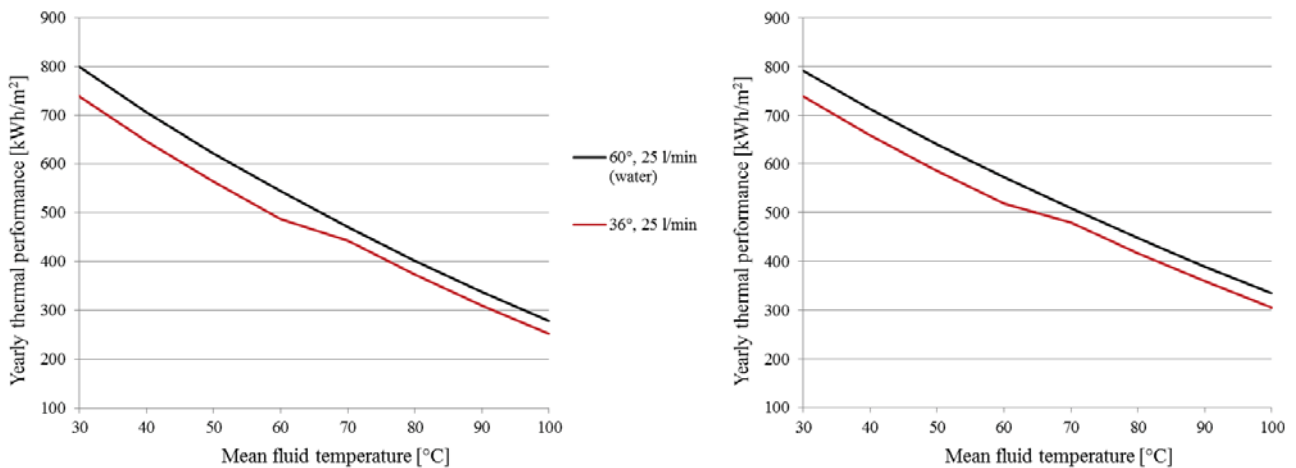

Figure 5.3: Yearly thermal performance for the collector HT-A (left) and HT-SA (right) according to the new Danish DRY for the radiation zone A.
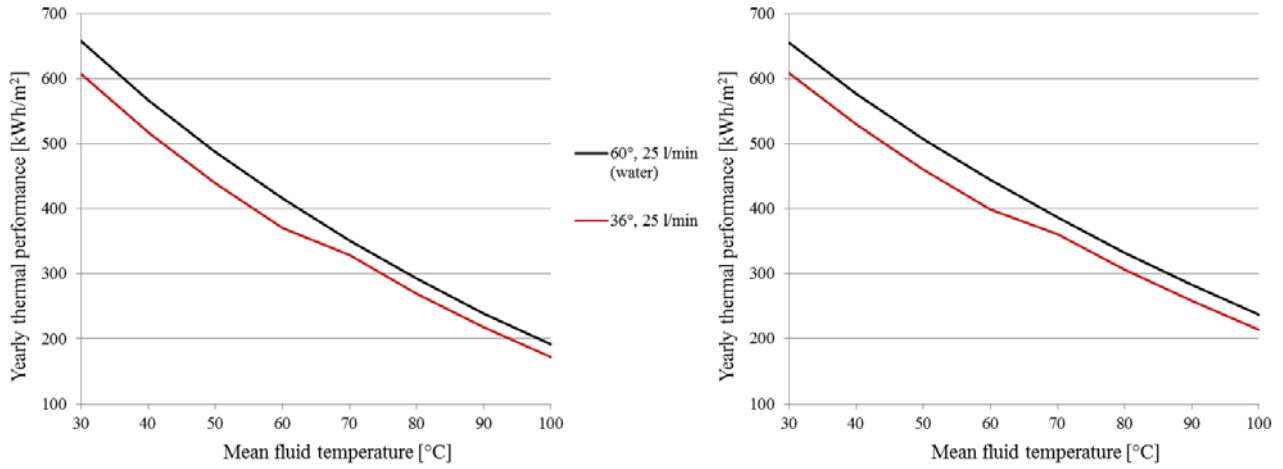
Figure 5.4: Yearly thermal performance for the collector HT-A (left) and HT-SA (right) according to the new Danish DRY for the radiation zone D.

In order to better quantify the effect caused by using the collector datasheet efficiency instead of real-world operating conditions, it was decided to calculate the ratio between the two curves shown in each of the diagrams represented in Figures 5.3 and 5.4. This ratio between the yearly thermal performance in real-world operating conditions and that calculated assuming data sheet efficiency gives information on the error which can be expected when predicting the energy output of a collector field based on data sheet efficiency. This performance ratio is shown in Figure 5.5 as function of the mean fluid temperature.
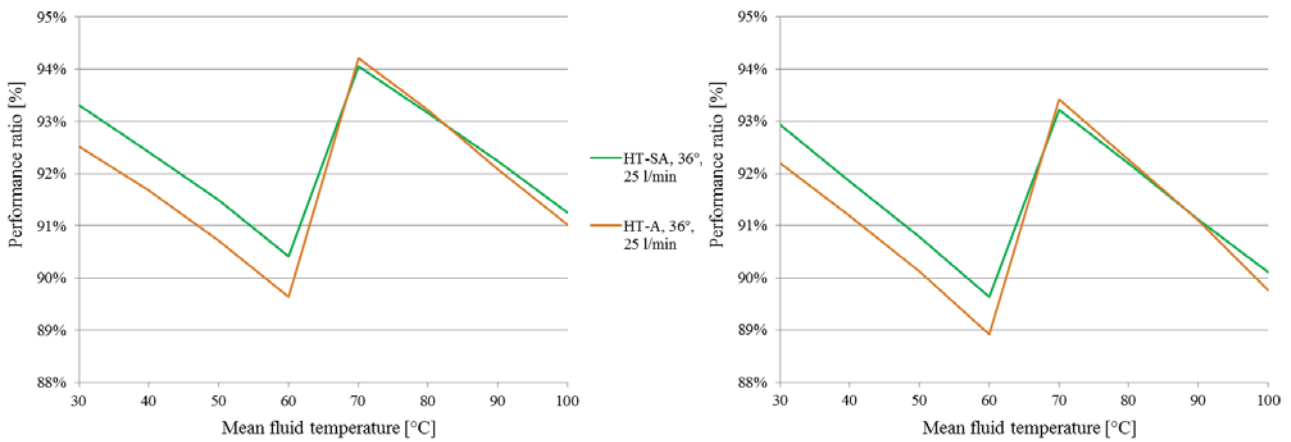
Figure 5.5: Performance ratio of the HT collectors with respect to datasheet conditions (100%) for radiation zone A (left) and D (right).

Figures 5.3 and 5.4 show that the larger differences occurred when the combination of fluid type, fluid flow rate and temperature entailed a different flow regime between the two cases being compared. For example, when the flow rate of the glycol/water mixture was equal to 25 litres min⁻¹ and the mean

temperature was larger than 65 °C, the flow regime was turbulent as for water: in this case the difference between the two yearly thermal performances was approximately 25 kWh m^{-2}, value which remained almost constant with the temperature level. On the other hand, the relative deviation increased with the temperature, as the yearly thermal performance became lower. When the glycol/water mixture was in laminar regime and water was in turbulent regime, the difference in thermal performance was approximately twice higher in absolute terms. Also in this case the relative difference increased with the temperature level, due to the lower yearly heat production. So, it can be concluded that almost half of the difference between the real-world operation curves and the corresponding curves obtained using data sheet efficiency was caused by the different flow regime in the two cases. The other half of the difference was due to the combined effect of different fluid and tilt angle, which both favoured the case where data sheet conditions were assumed. The overestimation of the yearly thermal performance caused by using efficiency expressions for water and for a collector tilt of 60° instead of a 40% glycol/water mixture at 36° tilt was in the range 6%-11%

Diagrams similar to those in Figures 5.3 and 5.4 are presented in Figures 5.6-5.12 for the old DRY as well as for all six radiation zones of the new DRY. A wider variety of flow rates and tilt angles was considered in this case. Regarding the tilt angle, the values of 30° and 45° were chosen because they represent the typical upper and lower threshold in Danish solar collector fields.

In each of the diagrams shown in Figures 5.6-5.12 the yearly thermal performance is presented for six different operating conditions, which are listed in Table 5.1. Four cases used 40% glycol/water mixture, as this is the fluid most commonly used in real-world applications, flow rates of 10 and 25 litres min^{-1} and tilt angles of 30° and 45°. In these four cases, the tilt angles to which the efficiency expressions refer to are the same as those assumed for the collector inclination. On the other hand, the other two cases used data sheet efficiency condition, which means water as solar collector fluid, 25 litres min^{-1} flow rate and 60° tilt, while collector tilts of 30° and 45° were actually assumed as collector tilt. In this way, a more direct comparison between the yearly thermal performance based on data sheet efficiency and that based on real-world operation conditions can be done.

The efficiency equations used in all six cases are those returned by Soleff models and listed in Tables 4.1 and 4.2 in section 4.3.

Table 5.1: Operating conditions assumed for yearly thermal performance calculations.

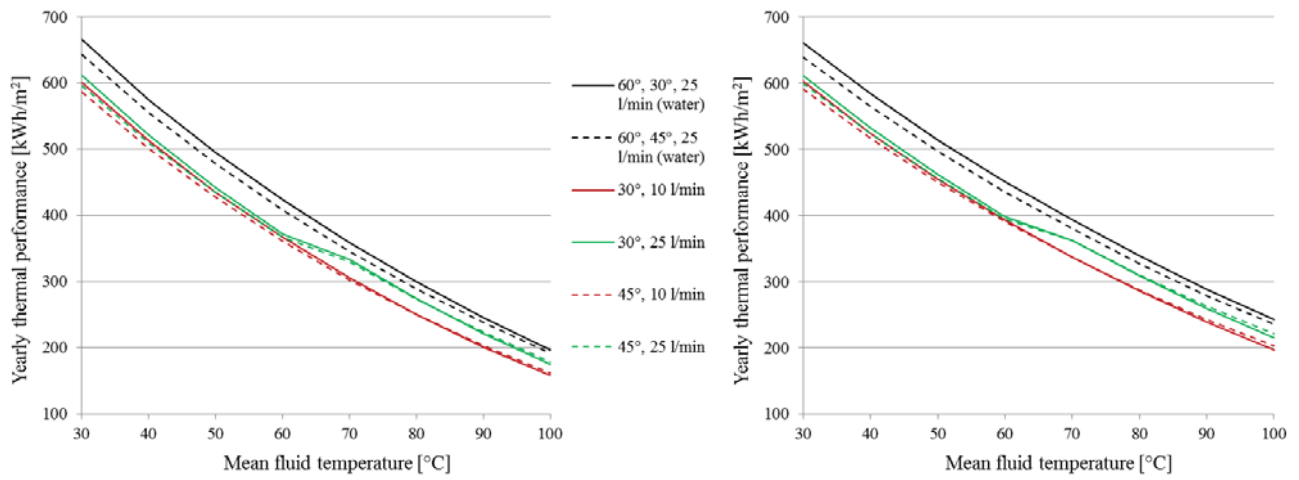| Fluid type	Flow rate [litres min^{-1}]	Efficiency tilt [°]	Collector tilt [°]
water	25	60	30
water	25	60	45
40% glycol	10	30	30
40% glycol	25	30	30
40% glycol	10	45	45
40% glycol	25	45	45

Figure 5.6: Yearly thermal performance for the collector HT-A (left) and HT-SA (right) according to the old Danish DRY.
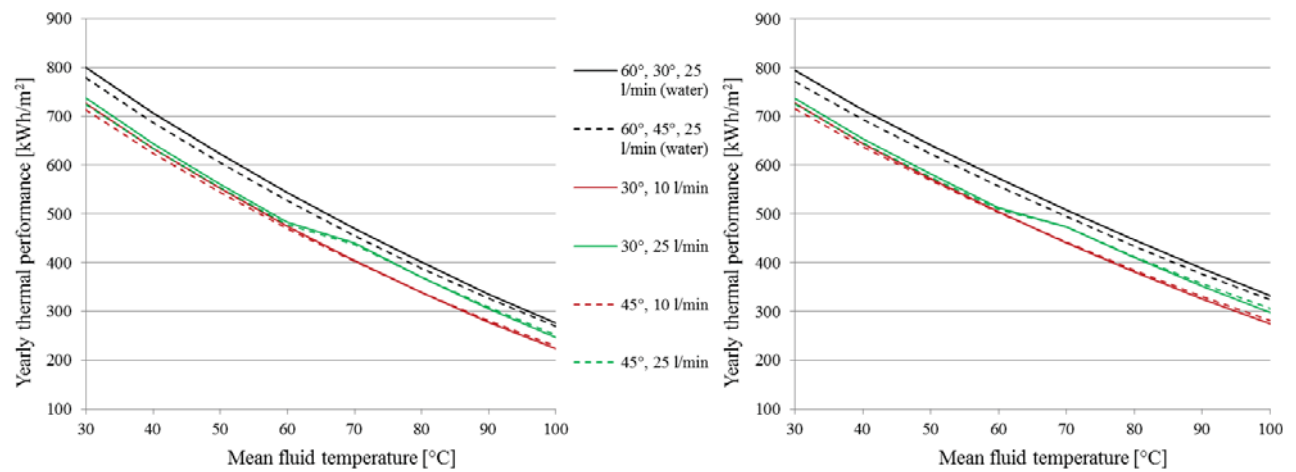

Figure 5.7: Yearly thermal performance for the collector HT-A (left) and HT-SA (right) according to the new Danish DRY for the radiation zone A.
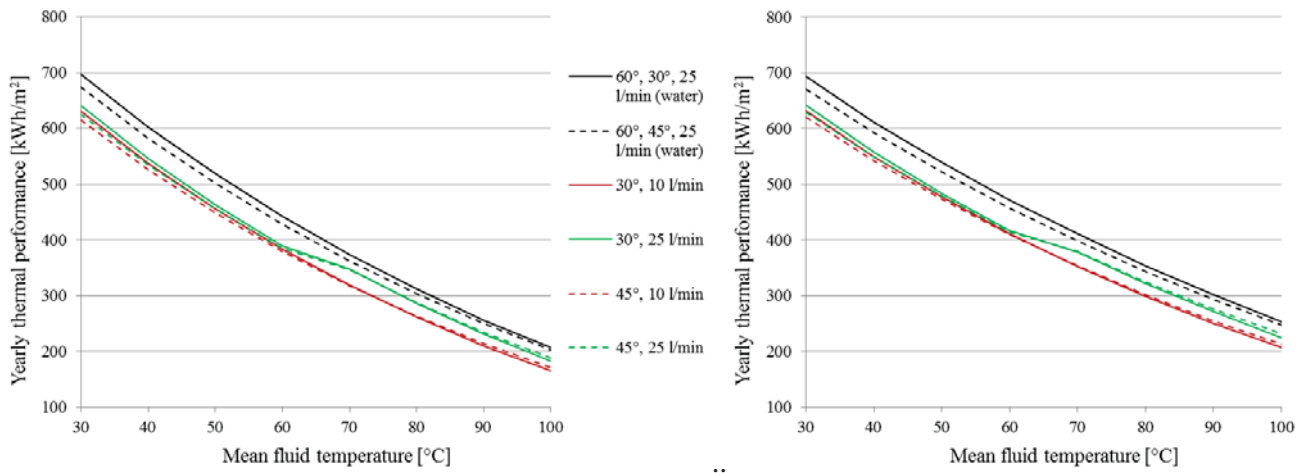
Figure 5.8: Yearly thermal performance for the collector HT-A (left) and HT-SA (right) according to the new Danish DRY for the radiation zone B.
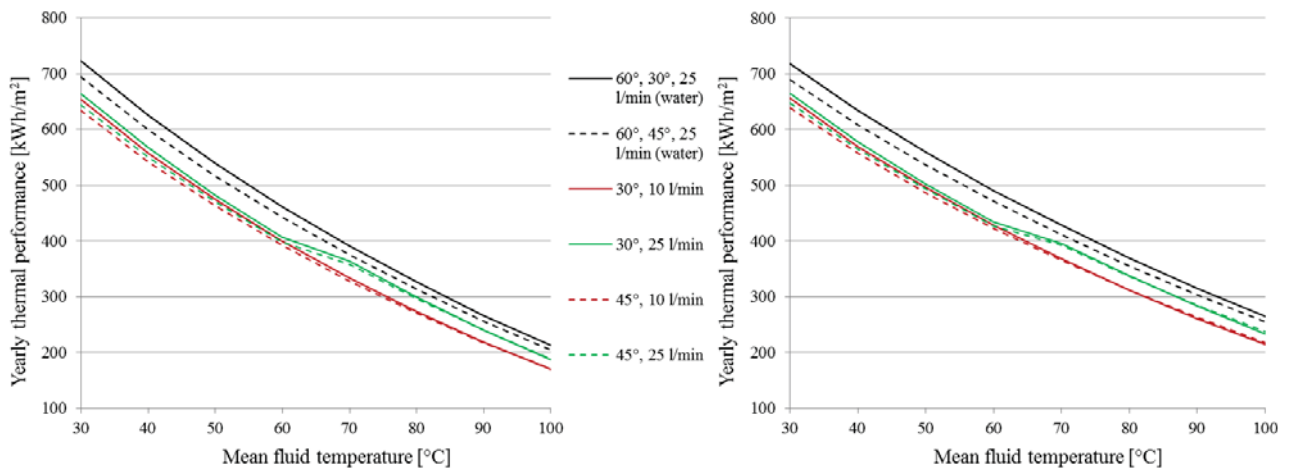

Figure 5.9: Yearly thermal performance for the collector HT-A (left) and HT-SA (right) according to the new Danish DRY for the radiation zone C.
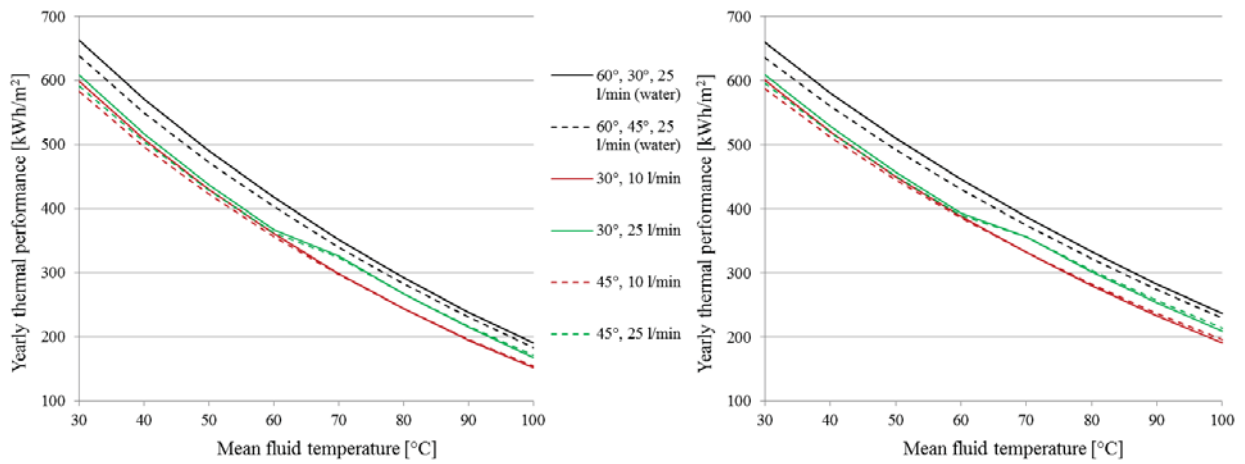
Figure 5.10: Yearly thermal performance for the collector HT-A (left) and HT-SA (right) according to the new Danish DRY for the radiation zone D.
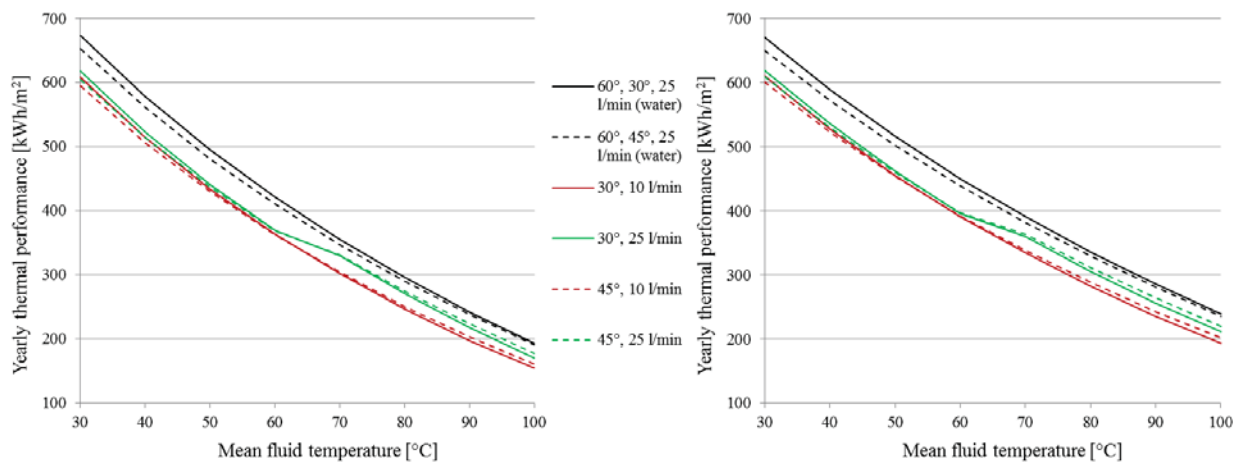

Figure 5.11: Yearly thermal performance for the collector HT-A (left) and HT-SA (right) according to the new Danish DRY for the radiation zone E.
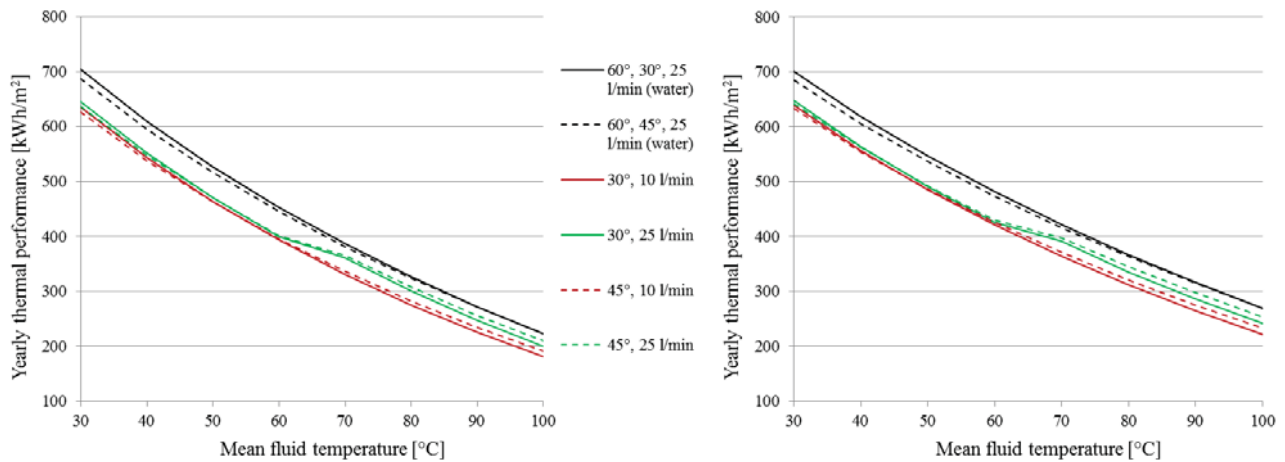
Figure 5.12: Yearly thermal performance for the collector HT-A (left) and HT-SA (right) according to the new Danish DRY for the radiation zone F.

First conclusion which can be drawn comparing Figure 5.6 to Figures 5.7-5.12 is that the old DRY is generally characterized by a lower solar radiation (and consequently lower yearly thermal performance) compared to the new ones. In fact, only the two radiation zones from the new DRY with the lowest solar radiation (zones D and E) gave comparable results with the old DRY, while the other four zones were characterized by noticeably better performances. This is in agreement with a general trend observed in Denmark that solar radiation has been increasing in the last years.

Comparing the new DRYs to each other, it can be seen that Bornholm was the zone giving the highest yearly thermal performance, thanks to the available solar radiation, which is almost 9% higher than the average value of the other five zones both on a 30° and 45° tilted surface.

As previously seen in Figures 5.3 and 5.4, also in Figures 5.6 and 5.12 the assumption of data sheet collector efficiencies caused an overestimation of the yearly thermal performance between 6% and 11%. Especially the flow regime played an important role in the offset between the curves.

Chapter 6: Conclusions and recommendation for future test standards for solar collectors

Investigations of different flat plate solar collectors showed that the solar collector efficiency is influenced by the solar collector fluid, the collector tilt and the volume flow rate. The collector efficiency is increased by:

- decreasing the percentage of glycol of the glycol/water mixture used as solar collector fluid
- increasing the collector tilt
- increasing the volume flow rate

It has been shown that flow regime (laminar or turbulent) has an important influence on both the thermal performance of a liquid-heating collector and on the ability to accurately predict collector performance. Differences between predicted efficiency based on current standard test conditions and actual performance in the field can be expected to be in the range of 6 to 11 %. It is therefore recommended that test conditions used by test institutes under collector tests are as close as possible to the conditions used under operation of the solar collectors.

Solar collectors should be designed and manufactured already thinking which kind of fluid, flow rates and temperatures they will be operated at, so that the absorber pipes can be properly sized to achieve turbulent conditions most of the times. To achieve this goal, the Reynolds number in the pipes should be larger than 4000. If the fluid type and the range of flow rates which will be used in the solar collector loop are known, it is possible to calculate the diameter of the absorber pipes which guarantees turbulence. This recommended diameter can be calculated through equation (Eq. 6.1), making explicit the correlation defining the Reynolds number.

$$D = \frac{4V'}{\mathrm{Re}\,\pi\,n\,\nu} \qquad \text{(Eq. 6.1)}$$

where D [m] is the recommended pipe diameter for the absorber pipes,

V' [m^3 s^{-1}] is the fluid flow rate through to the collector,

Re [-] is the desired Reynolds number (Re=4000),

n [-] is the number of parallel absorber pipes,

ν [m^2 s^{-1}] is the kinematic viscosity of the collector fluid, which should be provided by the manufacturer

Regarding (Eq. 6.1), a uniform flow distribution is assumed. This is obviously a simplification, but can be considered acceptable for large solar collectors like ARCON HT models. In fact, in this case the

absorber pipes are much longer and thinner than the manifolds, so that they are responsible for most of the pressure drop across the collector. Another consideration is that, as the viscosity decreases strongly with the temperature, also the recommended diameter will vary. In practise, the diameter should be calculated from (Eq. 6.1) assuming the lowest temperature which is expected in the collector loop, so that turbulence is achieved for any other operation temperature. For similar reasons, also the flow rate used for the calculation should be the lowest operation flow rate which is expected to be used. After calculating the recommended diameter, it is advisable to check that the consequent pressure losses are acceptable.

Concerning the procedure to measure the efficiency, changes in flow regime within the investigated temperature range should be avoided, as they would affect the trend of the interpolating curve. Only single efficiency points which are characterized by the same flow regime should be interpolated. In case the transition from laminar to turbulent condition occurs at a temperature lower than the operation temperature range at which the collector operates at, then the efficiency curve could be obtained only considering the relevant temperature interval, neglecting the lower temperature level where transition occurs. In this way, a better fit can be obtained without loss of relevant information. Large solar collectors for district heating application can be an example. In such installation the inlet temperature to the collector field is approximately equal to the return temperature from the district heating network (40-50 °C). Consequently, it is not particularly relevant to investigate the collector efficiency for lower temperatures.

References

Arcon Solar A/S, 2010. ARCON solfanger - type HT-SA 35/10.

Chiou, J. P., 1982. The effect of non-uniform fluid flow distribution on the thermal performance of solar collector. Solar Energy 6, 487-502.

Danmarks Meteorologiske Institut (DMI), 2012. Technical Report 12-17: 2001–2010 Design Reference Year for Denmark.

Fan, J., Furbo, S., 2008. Buoyancy effects on thermal behavior of a flat-plate solar collector. Journal of Solar Energy Engineering 130.

Furbo, S., Holck, O., 1995. Efficiencies of solar collectors for different tilts. Measurements. Report SR 95-7, Thermal Insulation Laboratory, Technical University of Denmark.

Furbo, S., Perers, B., Bava, F., 2014. Thermal performance of solar district heating plants in Denmark, in EuroSun 2014 Conference Proceedings, Aix-les-Bains, France.

Furbo, S., Shah L.J., 2003. Thermal advantages for solar heating systems with a glass cover with antireflection surfaces. Solar Energy 74, 513-523.

Idelchik, I.E., 1994. Handbook of hydraulic resistance, third ed. CRC press.

SP Technical Research Institute of Sweden, 2011. Technical Report Ref. PX12871-01.

Rasmussen, P.B., Svendsen, S., 1996. SolEff Program til beregning af solfangeres effektivitet. Thermal Insulation Laboratory, Technical University of Denmark.

Wang, X. A., Wu, L. G., 1990. Analysis and performance of flat plate solar collector arrays. Solar Energy 2, 71-78.

Investigations on the efficiencies of different flat plate solar collectors have been carried out in an indoor test facility at EXOVA, Canada and an outdoor test facility at the Technical University of Denmark. The investigations showed that the solar collector efficiency is influenced by the solar collector fluid, the collector tilt and the volume flow rate. The collector efficiency is increased by:

  - Decreasing the percentage of glycol of the glycol/water mixture used as solar collector fluid
  - Increasing the collector tilt
  - Increasing the volume flow rate